bioRxiv preprint doi: https://doi.org/10.1101/735449; this version posted August 14, 2019. The copyright holder for this preprint (which was not certified by peer review) is the author/funder, who has granted bioRxiv a license to display the preprint in perpetuity. It is made available under aCC-BY 4.0 International license.

Cholinergic-like neurons carrying PSEN1 E280A mutation from familial Alzheimer's disease reveal intraneuronal Aβ42 peptide accumulation, hyperphosphorylation of TAU, oxidative stress, apoptosis and Ca2+ flux dysregulation: Therapeutic Implications

Viviana Soto-Mercado[1], Miguel Mendivil-Perez[1], Carlos Velez-Pardo [1], Francisco Lopera[1], Marlene Jimenez-Del-Rio[1,*]

[1]Neuroscience Research Group, Medical Research Institute, Faculty of Medicine, University of Antioquia (UdeA), Calle 70 No. 52-21, and Calle 62 # 52-59, Building 1, Room 412; SIU Medellin, Colombia

*Correspondence to Jimenez-Del-Rio M, email: marlene.jimenez@udea.edu.co;

ORCID # 0000-0003-3477-2386

Carlos Velez-Pardo ORCID # 0000-0002-0557-0411

bioRxiv preprint doi: https://doi.org/10.1101/735449; this version posted August 14, 2019. The copyright holder for this preprint (which was not certified by peer review) is the author/funder, who has granted bioRxiv a license to display the preprint in perpetuity. It is made available under aCC-BY 4.0 International license.

Abstract

Alzheimer's disease (AD) is a neurodegenerative disorder characterized by progressive memory loss and cognitive disturbance as a consequence of the loss of cholinergic neurons in the brain, neuritic plaques and hyperphosphorylation of TAU protein. Although the underlying mechanisms leading to these events are unclear, mutations in presenilin 1 (PSEN1), e.g., E280A (PSEN1 E280A), are causative factors for autosomal dominant early-onset familial AD (FAD). Despite advances in the understanding of the physiopathology of AD, there are no efficient therapies to date. Limitations in culturing brain-derived live neurons might explain the limited effectiveness of AD research. Here, we show that mesenchymal stromal (stem) cells (MSCs) can be used to model FAD, providing novel opportunities to study cellular mechanisms and to establish therapeutic strategies. Indeed, we cultured MSCs with the FAD mutation PSEN1 E280A and wild-type (WT) PSEN1 from umbilical cords and characterized the transdifferentiation of these cells into cholinergic-like neurons (ChLNs). PSEN1 E280A ChLNs but not WT PSEN1 ChLNs exhibited increased intra- and extracellular Aβ42 peptide and TAU phosphorylation (at residues Ser202/Thr205), recapitulating the molecular pathogenesis of FAD caused by mutant PSEN1. Furthermore, PSEN1 E280A ChLNs presented oxidative stress (OS) as evidenced by the oxidation of DJ-1Cys106-SH into DJ-1Cys106-SO3 and the detection of DCF-positive cells and apoptosis markers such as activated pro-apoptosis proteins p53, c-JUN, PUMA and CASPASE-3 and the concomitant loss of the mitochondrial membrane potential and DNA fragmentation. Additionally, mutant ChLNs displayed Ca2+ flux dysregulation and deficient acetylcholinesterase (AChE) activity compared to control ChLNs. Interestingly, the inhibitor JNK SP600125 almost completely blocked TAU phosphorylation. Our findings demonstrate that FAD MSC-derived cholinergic neurons

bioRxiv preprint doi: https://doi.org/10.1101/735449; this version posted August 14, 2019. The copyright holder for this preprint (which was not certified by peer review) is the author/funder, who has granted bioRxiv a license to display the preprint in perpetuity. It is made available under aCC-BY 4.0 International license.

with the PSEN1 E280A mutation are a valid model of AD and provide important clues for the identification of targetable pathological molecules.

Keywords

Cholinergic neurons; mesenchymal stromal cells; familial Alzheimer disease; PSEN1; E280A mutation; $A\beta_{1-42}$, TAU, oxidative stress, apoptosis, neuronal dysfunction.

bioRxiv preprint doi: https://doi.org/10.1101/735449; this version posted August 14, 2019. The copyright holder for this preprint (which was not certified by peer review) is the author/funder, who has granted bioRxiv a license to display the preprint in perpetuity. It is made available under aCC-BY 4.0 International license.

Introduction

Alzheimer's disease (AD) is a chronic neurodegenerative condition characterized by loss of memory, reasoning and decision-making functions [1] due to the severe loss of cholinergic neurons from the nucleus basalis magnocellularis of Meynert and cholinergic projections to the cortex and hippocampus [2]. The neuropathological profile of AD is associated with the extracellular accumulation of insoluble forms of amyloid-β (Aβ) in plaques and intracellular aggregation of the microtubule protein TAU in neurofibrillary tangles [3]. Aβ is derived by the proteolytic cleavage of amyloid β precursor protein (APP). APP is first cleaved by β-secretase, which then undergoes additional cleavages by γ-secretase to generate a series of peptides prone to aggregation. Most mutations in the presenilin 1 (*PSEN 1)* gene, which codes for the catalytic component of γ-secretase [4], result in the overproduction of Aβ, specifically, the 42-amino acid Aβ isoform ($A\beta_{1-42}$, hereafter $A\beta_{42}$) [5], and occur most frequently in familial AD (FAD; http://www.molgen.ua.ac.be/ADMutations/). Glu280Ala (p. E280A, c.839A > C, exon 8) in *PSEN1* is a well-characterized FAD mutation found in a large kindred localized in Antioquia, Colombia [6-9] that shows typical phenotypes of AD with complete penetrance [10]. Similar to the majority of dominant-negative *PSEN1* mutations [11, 12], PSEN1 E280A produces increased $A\beta_{42}$ deposition [13], hippocampal neuron loss [14], and Aβ/ TAU accumulation in young adults [15, 16].

Despite advances in the understanding of the physiopathology of AD [17], there are no efficient therapies to date. Although limitations in culturing brain-derived live neurons might slow AD research, the rapid advances in cellular genetic reprogramming, in

bioRxiv preprint doi: https://doi.org/10.1101/735449; this version posted August 14, 2019. The copyright holder for this preprint (which was not certified by peer review) is the author/funder, who has granted bioRxiv a license to display the preprint in perpetuity. It is made available under aCC-BY 4.0 International license.

particular the induction of somatic cells (e.g., fibroblast) into stem cells (e.g., human induced pluripotent stem cells, hiPSCs), has led to the modeling of FAD PSEN1 mutations *in vitro* [18-21]. Obtaining iPSCs from patients bearing *PSEN1* mutations is appealing; however, the isolation and purification procedures are technically challenging, expensive, time consuming and labor intensive. Alternatively, the human mesenchymal stromal (stem) cells derived from Wharton's jelly tissue (WJ-MSCs) are multipotent cells that can differentiate and/or transdifferentiate into mesodermal and ectodermal lineage cells [22-25]. Because MSCs might be equivalent to human embryonic stem cells (hESCs) and hiPSCs [26, 27], these cells have become an interesting and promising tool for modeling FAD PSEN1 E280A *in vitro.*

The aim of the present study was to establish an *in vitro* cellular model that reveals the major pathologic features of the FAD PSEN1 E280A mutation, thereby enabling investigation of the pathomechanisms of early onset FAD. Therefore, $A\beta_{42}$ production, TAU phosphorylation, oxidative stress (OS), cell death, and neuronal dysfunction were investigated in cholinergic-like neurons (ChLNs) derived from wild-type (control) and PSEN1 E280A MSCs. We demonstrate for the first time that FAD PSEN1 E280A pathology can be recapitulated in MSC-derived ChLNs. These findings in ChLNs show great promise for modeling human FAD *in vitro* and identifying therapeutic targets for AD treatment.

bioRxiv preprint doi: https://doi.org/10.1101/735449; this version posted August 14, 2019. The copyright holder for this preprint (which was not certified by peer review) is the author/funder, who has granted bioRxiv a license to display the preprint in perpetuity. It is made available under aCC-BY 4.0 International license.

Materials and Methods

The collection and use of umbilical cords from newborns were approved by the Ethics Committee of the Sede de Investigacion Universitaria-SIU-, University of Antioquia, and the Medical Ethics Committee of Hospital San Juan de Dios, Yarumal, Colombia and were provided following natural childbirth with written consent. Donors had a familial background of AD. The mother's medical history was negative for human pathogens, such as human immunodeficiency virus 1/2, hepatitis B and C virus, and syphilis. The cord (~7 cm long) was immersed in low-glucose DMEM (Sigma) supplemented with 100 U Penicillin/streptomycin (Sigma) and 5 µg/ml Plasmocin (Invivogen) and immediately transported to the laboratory.

Isolation and Expansion of hWJ-MSCs

The human umbilical cords were obtained from ten healthy, natural childbirths (Tissue Bank Code (TBC) # WJMSC-11, -12, -13, -14, -15, -16, -17, -18, -19, -20) and aseptically stored at 4 °C PBS containing 1% penicillin and streptomycin. The cords were rinsed several times to drain blood from vessels, cut into 2–3-cm-long segments and rinsed again. Umbilical arteries and veins were removed, and the remaining tissue was transferred to a sterile container and chopped into small fragments in PBS. The explants were digested with an enzyme mixture containing 0.25% trypsin, 0.1% Dispase and 0.5% collagenase II for 2 h at 37 ºC under constant agitation. Then, the digestion products were centrifuged at 2,000 rpm for 40 min, and the pellet was cultured in T75 cell culture flasks (Corning) in hWJ-MSC regular culture medium (low-glucose DMEM supplemented with 20% fetal bovine serum (FBS, Sigma), 100 U penicillin/ streptomycin and 5 µg/ml Plasmocin). Once confluence had been reached, adherent cells (passage 0) were detached with 0.25% trypsin

bioRxiv preprint doi: https://doi.org/10.1101/735449; this version posted August 14, 2019. The copyright holder for this preprint (which was not certified by peer review) is the author/funder, who has granted bioRxiv a license to display the preprint in perpetuity. It is made available under aCC-BY 4.0 International license.

and passaged at 13,000 cells/ cm^2 in a T75 flask. Cells from passages 2 or 4 were harvested during the first expansion period for further characterization and cryopreservation.

Identification of the PSEN1 E280A mutation

The PSEN1 E280A mutation was detected by PCR using mismatch primers and digestion of the products with *Bsm1* [28]. Digested products were separated on a 3% agarose gel. According to the electrophoretic patterns, the samples were classified as wild-type (WT) or mutant PSEN1 E280A. Based on this classification, the TBC# WJMSC-11 WT PSEN1 and TBC# WJMSC-12 PSEN1 E280A cell lines were selected for further experiments.

APOE genotyping analysis

Genotyping of the APOE polymorphism was performed using polymerase chain reaction amplification of a 244-bp fragment followed by digestion with *HhaI* as described by [29].

Karyotyping

Karyotype analysis was performed by the Medical Genetics Unit of the Faculty of Medicine, UdeA, using standard cytogenetic protocols. At 60-70% confluence, WJMSC-11 WT and WJMSC-12 PSEN1 E280A cells were incubated with 0.1 mg/ml Colcemid (Sigma) for 90 min at 37 °C. Then, the cells were detached with 0.25% trypsin and centrifuged at 2,300 RPM for 20 min. The medium was removed, and the hypotonic solution (0.075 M KCl, 0.017 M Na-citrate) was added and incubated for 20 min at 37 °C. After a new centrifugation, cells were fixed with freshly prepared Carnoy's solution. Metaphase spreads were analyzed after staining with quinacrine (Sigma) for karyotyping. Analysis was performed on three different primary cultures counting 20 metaphases for each sample.

bioRxiv preprint doi: https://doi.org/10.1101/735449; this version posted August 14, 2019. The copyright holder for this preprint (which was not certified by peer review) is the author/funder, who has granted bioRxiv a license to display the preprint in perpetuity. It is made available under aCC-BY 4.0 International license.

Colony-forming units assay

The colony formation assay is an *in vitro* cell survival assay based on the ability of a single cell to grow into a colony [30]. WJMSC-11 WT and WJMSC-12 PSEN1 E280A cells were seeded at a density of 200 cells/ well on 6-well plates followed by the addition of 3 mL of regular culture medium. The cultures were left to grow in a humidified atmosphere with 5% CO_2 at 37 °C for 15 days. The culture medium was changed twice a week. After 15 days of cultivation, both WT and mutant PSEN-1 cells were stained with 0.5% crystal violet and counted using the cell counter plugin from ImageJ program. The experiment was conducted three times.

Immuno-phenotypic characterization

Standard flow cytometry techniques were used to determine the cell surface epitope profile (CD9, CD73, CD90, CD34 and CD45) of both WT and mutant PSEN1 MSCs. Briefly, hWJ-MSCs were incubated with saturating concentrations (1:500) of mouse monoclonal antibodies conjugated to human CD9-peridinin chlorophyll protein (PerCP)-cy5.5, CD73-phycoerythrin (PE), CD90 PE-cy5.5, CD34 PE, and CD45- fluorescein isothiocyanate (FITC). All antibodies were purchased from BD Biosciences (San Diego, CA). Cells were incubated for 1 h at 4 °C. Prior to antibody labeling, the cells were preincubated with 5% fetal bovine sera (FBS) for 10 min to block nonspecific binding. Cell suspensions were washed and resuspended in PBS for analysis on an LSRFortessa (BD Biosciences). Ten thousand events were acquired, and the acquisition analysis was performed using FlowJo 7.6.2. Positive staining was defined as the fluorescence emission that exceeded levels obtained by more than 99% of cells from the population stained with the corresponding

bioRxiv preprint doi: https://doi.org/10.1101/735449; this version posted August 14, 2019. The copyright holder for this preprint (which was not certified by peer review) is the author/funder, who has granted bioRxiv a license to display the preprint in perpetuity. It is made available under aCC-BY 4.0 International license.

negative controls. The isotype (negative) control used in this study was IgG1 PE-Cy5.5, IgG1-PE and IgG1- FITC (BD Biosciences).

Cell differentiation

Adipogenic differentiation

Adipogenic differentiation was performed according to [31] with minor modifications. Briefly, WT and mutant MSCs at passages 4-7 were plated at a density 20,000 cells/cm^2 in a 12-well plate in regular culture medium. At 90–100% confluence, the culture medium was replaced by adipogenic induction medium, including high-glucose DMEM, 10% FBS, 0.5 mM 3-isobutyl-1-methylxanthine (Sigma, cat # I5879), 100 µM indomethacin (Sigma, cat # I7378), 0.1 µM dexamethasone and 10 µg/ mL insulin. After 28 days, cells were fixed with 4% formaldehyde (FA) and immediately stained with the standard Oil-Red-O protocol. Control cells were kept in regular culture medium.

Osteogenic differentiation

Osteogenic differentiation was performed according to [31] with minor modifications. Briefly, WT and mutant cells at passages 4-7 were plated at a density of 10,000 cells/ cm^2 in 12-well plates in regular culture medium. After 72 h, the culture medium was replaced by osteogenic differentiation medium containing high-glucose DMEM (Sigma), 10% FBS, 1 µM dexamethasone (Alfa Aesar, cat # A17590), 250 µM sodium ascorbate (Sigma, cat # A4034), and 10 mM β-glycerophosphate (Alfa Aesar, cat # L03425). The medium was changed every 3-4 days. Control cells were kept in regular culture medium. After 28 days of induction, cells were fixed in 4% FA and stained with standard Von Kossa Staining.

Chondrogenic differentiation

Chondrogenic differentiation was performed according to [32] with minor modifications. Briefly, 2.5×10^5 WT and mutant cells were left aggregated in microwell plates and then

bioRxiv preprint doi: https://doi.org/10.1101/735449; this version posted August 14, 2019. The copyright holder for this preprint (which was not certified by peer review) is the author/funder, who has granted bioRxiv a license to display the preprint in perpetuity. It is made available under aCC-BY 4.0 International license.

provided with chondrogenic medium containing high-glucose DMEM, 10% FBS, 10 µg/ L TGF-β3, 0.1 µmol/ L dexamethasone, 50 µmol/ L vitamin C, and 6.25 mg/L insulin. The medium was changed every 3-4 days. Control cells were kept in regular culture medium. After 28 days of induction, cells were fixed in 4% formaldehyde, stained with toluidine blue for 2 min at room temperature and viewed by light microscopy.

Cholinergic-like neuron (ChLN) differentiation

ChLN differentiation was performed according to [25]. WT and mutant MSCs were seeded at 1-1.5 x 10^4 cells/ cm^2 in laminin-treated culture plates for 24 h in regular culture medium. Then, the medium was removed, and cells were incubated in minimal culture medium (hereafter MCm) containing low-glucose DMEM and 1% FBS or in cholinergic differentiation medium (*Cholinergic-N-Run medium*, hereafter Ch-N-Rm) containing DMEM/F-12 media 1:1 Nutrient Mixture (Gibco cat# 10565018), 10 ng/ mL basic fibroblast growth factor (bFGF) recombinant human protein (Gibco Cat# 13256029), 50 µg/ mL sodium heparin (Hep, Sigma-Aldrich cat# H3393), 0.5 µM all-trans retinoic acid, 50 ng/ml sonic hedgehog peptide (SHH, Sigma cat# SRP3156) and 1% FBS at 37 °C for 7 days. After this process of transdifferentiation, the cells were labeled as WT PSEN1 or PSEN1 E280A ChLNs.

Immunofluorescence analysis

For the analysis of neural-, Alzheimer's disease-, oxidative stress- and cell death-related markers, the cells treated under different conditions were fixed with cold ethanol (-20 °C) for 20 min, followed by Triton X-100 (0.1%) permeabilization and 10% bovine serum albumin (BSA) blockage. Cells were incubated overnight with primary neural antibodies against glial fibrillary acidic protein (GFAP 1:200, cat# sc6170, Santa Cruz), microtubule-associated protein 2 (MAP2, 1:250, cat MA1-25044, Invitrogen), β-tubulin III (1:250, cat#

bioRxiv preprint doi: https://doi.org/10.1101/735449; this version posted August 14, 2019. The copyright holder for this preprint (which was not certified by peer review) is the author/funder, who has granted bioRxiv a license to display the preprint in perpetuity. It is made available under aCC-BY 4.0 International license.

G712 A, Promega) and choline-acetyltransferase (ChAT, 1:50, cat# AB144 P, Millipore); primary antibodies against protein amyloid $\beta_{1\text{-}42}$ (1:500; $A\beta_{1\text{-}42}$ cat# AB5078P, Sigma-Aldrich), total TAU (1: 500; t-Tau; cat# T6402, Sigma), and phospho-TAU (p-Tau, 1:500, Ser202/Thr205, cat# MN1020 (AT8), Thermo Fisher Scientific); and primary antibodies against oxidized DJ-1 (1:500; ox(Cys106)DJ1; spanning residue C^{106} of human PARK7/DJ1; oxidized to produce cysteine sulfonic (SO_3) acid; cat # MABN1773, Millipore). To assess cell death, we used primary antibodies against p53-upregulated modulator of apoptosis (1:500; PUMA, cat# ab-9643, Abcam), p53 (1:500; cat# MA5-12453, Millipore), phospho-c-Jun (1:250; c-Jun (S63/73) cat# sc-16312, Santa Cruz), and caspase-3 (1:250; cat # AB3623, Millipore). After exhaustive rinsing, we incubated the cells with secondary fluorescent antibodies (DyLight 488 and 594 horse anti-rabbit, -goat and -mouse, cat DI 1094, DI 3088, and DI 2488, respectively) at 1:500. The nuclei were stained with 1 µM Hoechst 33342 (Life Technologies), and images were acquired on a Floyd Cells Imaging Station microscope.

Western blot analysis

Cells were incubated as described above, detached with 0.25% trypsin and lysed in 50 mM Tris-HCl, pH 8.0, with 150 mM sodium chloride, 1.0% Igepal CA-630 (NP-40), and 0.1% sodium dodecyl sulfate and a protease inhibitor cocktail (Sigma-Aldrich). All lysates were quantified using the bicinchoninic acid assay (Thermo Scientific cat # 23225). Extracted samples (30 µg of proteins) were heated at 95 °C for 5 min in 2 x SDS and 20x reducing agent (except for protein oxDJ-1) and loaded into 12% Bis/Tris gels at 120 V for 90 min, and the bands were transferred onto nitrocellulose membranes (Hybond-ECL, Amersham Biosciences) at 270 mA for 90 min using an electrophoretic transfer system (BIO-RAD)

bioRxiv preprint doi: https://doi.org/10.1101/735449; this version posted August 14, 2019. The copyright holder for this preprint (which was not certified by peer review) is the author/funder, who has granted bioRxiv a license to display the preprint in perpetuity. It is made available under aCC-BY 4.0 International license.

according to Sandoval et al. 2013 [33] with minor modifications. The membranes were incubated overnight at 4 °C with anti-GFAP, MAP2, β-tubulin III, ChAT, amyloid β_{1-42}, total TAU, phospho-TAU, ox(Cys^{106}) DJ1, PUMA, p53, p-c-Jun and caspase-3 primary antibodies (1:5000). The anti-actin antibody (1:1000, cat #MAB1501, Millipore) was used as an expression control. Secondary infrared antibodies (goat anti-rabbit IRDye® 680RD, cat #926-68071; donkey anti-goat IRDye ® 680RD, cat # 926-68074; and goat anti mouse IRDye ® 800CW, cat #926-32270; LI-CORBiosciences) at 1:1000 were used for western blotting analysis, and data were acquired using Odyssey software. To directly control the conformation-dependent differences among Aβ assemblies, we prepared a homogenous synthetic unaggregated (i.e., monomers) and large oligomeric Aβ42 assemblies according to Stine et al., 2011 [34]. Briefly, after solubilization of the peptide (Sigma Cat #A9810) in DMSO, the "unaggregated" peptide was obtained by dissolving the DMSO-solubilized peptide in water and used immediately (0 days). To obtain the "large oligomers", 10mM Tris was added to DMSO-solubilized peptide solution and incubated it for 15 days at 4 °C. The determination of the aggregation state of Aβ42 was performed by Western analysis of SDS-PAGE as described above. The assessment was repeated three times in independent experiments.

Evaluation of intracellular hydrogen peroxide (H_2O_2) by fluorescence microscopy

To determine the levels of intracellular H_2O_2, we used 2′,7′-dichlorofluorescein diacetate (5 μM, DCFH2-DA; Invitrogen). hWJ-MSCs or ChLNs were left in regular medium for 0, 2 and 4 days. Then, the cells ($5x10^3$) were incubated with the $DCFH_2$-DA reagent for 30 min at 37 °C in the dark. Cells were then washed, and DCF fluorescence intensity was determined by analysis of fluorescence microscopy images. The assessment was repeated

bioRxiv preprint doi: https://doi.org/10.1101/735449; this version posted August 14, 2019. The copyright holder for this preprint (which was not certified by peer review) is the author/funder, who has granted bioRxiv a license to display the preprint in perpetuity. It is made available under aCC-BY 4.0 International license.

three times in independent experiments. The nuclei were stained with 0.5 µM Hoechst 33342 (2.5 µM) staining compound. The assessment was repeated three times in independent experiments blind to experimenter.

Evaluation of intracellular hydrogen peroxide (H_2O_2) by flow cytometry

H_2O_2 was determined with 2',7'-dichlorofluorescein diacetate (1 µM, $DCFH_2$-DA). ChLNs were left in regular medium for 0, 2 and 4 days. Then, the cells (1×10^5) were incubated with $DCFH_2$-DA reagent for 30 min at 37 °C in the dark. Cells were then washed, and DCF fluorescence was determined using an LSRFortessa (BD Biosciences). The assessment was repeated 3 times in independent experiments. Quantitative data and figures were obtained using FlowJo 7.6.2 Data Analysis Software. The assessment was repeated three times in independent experiments blind to experimenter and flow cytometer analyst.

Analysis of mitochondrial membrane potential (ΔΨm) by fluorescence microscopy

The hWJ-MSCs or ChLNs were left in regular medium for 0, 2 and 4 days. Then, the cells ($5x10^3$) were incubated with the passively diffusing and active mitochondria-accumulating dye deep-red MitoTracker compound (20 nM, final concentration) for 20 min at RT in the dark (Invitrogen, cat # M22426). Cells were then washed twice with PBS. MitoTracker fluorescence intensity was determined by analysis of fluorescence microscopy images. The assessment was repeated three times in independent experiments. The nuclei were stained with 0.5 µM Hoechst 33342 (2.5 µM) staining compound. The assessment was repeated three times in independent experiments blind to experimenter and flow cytometer analyst.

Analysis of mitochondrial membrane potential (ΔΨm) by flow cytometry

ChLNs were left in regular medium for 0, 2 and 4 days. Then, the cells (1×10^5) were incubated for 30 min at RT in the dark with MitoTracker (20 nM, final concentration). The cells were analyzed using an LSRFortessa (BD Biosciences). The experiment was

bioRxiv preprint doi: https://doi.org/10.1101/735449; this version posted August 14, 2019. The copyright holder for this preprint (which was not certified by peer review) is the author/funder, who has granted bioRxiv a license to display the preprint in perpetuity. It is made available under aCC-BY 4.0 International license.

performed three times in independent experiments, and 10,000 events were acquired for analysis. Quantitative data and figures were obtained using FlowJo 7.6.2 Data Analysis Software. The assessment was repeated three times in independent experiments blind to experimenter and flow cytometer analyst.

Determination of DNA fragmentation by flow cytometry

DNA fragmentation was determined using a hypotonic solution of PI. Cells entering the cellular cycle phase sub-G_0 were identified as those undergoing apoptosis. ChLNs were left in regular medium for 0, 2 and 4 days. Then, the cells ($1x10^5$) were detached, washed twice with PBS (pH 7.2) and stored in 95% ethanol overnight at -20 °C. The cells were washed and incubated in 400 µL solution containing propidium iodide (PI; 50 µg/ml), RNase A (100 µg/ mL), EDTA (50 mM), and Triton X-100 (0.2%) for 60 min at 37 °C. The cell suspension was analyzed for PI fluorescence using an Epics XL flow cytometer (Beckman Coulter). DNA fragmentation was assessed 3 times in independent experiments. Quantitative data and figures from the sub-G_0/G_1 population were obtained using FlowJo 7.6.2 Data Analysis Software. The assessment was repeated three times in independent experiments blind to experimenter and flow cytometer analyst.

Acetylcholinesterase activity measurement

We determined the acetylcholinesterase (AChE) activity using the AChE Assay Kit (Abcam, Cat# ab138871) according to the manufacturer's protocol. Briefly, ChLNs at days 0, 2 and 4 post differentiation were detached with 0.25% trypsin and mechanically lysed by freezing/sonication. Lysates were centrifuged at 13,000 rpm for 15 min, and supernatants were used for protein quantification by the BCA method (see above) and the detection of AChE activity. AChE degrades the neurotransmitter acetylcholine (ACh) into choline and acetic acid. We used the DTNB (5,5′-dithiobis(2-nitrobenzoic acid)) reagent to quantify the

bioRxiv preprint doi: https://doi.org/10.1101/735449; this version posted August 14, 2019. The copyright holder for this preprint (which was not certified by peer review) is the author/funder, who has granted bioRxiv a license to display the preprint in perpetuity. It is made available under aCC-BY 4.0 International license.

thiocholine produced from the hydrolysis of acetylthiocholine by AChE. The absorption intensity of the DTNB adduct was used to measure the amount of thiocholine formed, which was proportional to AChE activity. We read the absorbance in a microplate reader at ~410 nm. The data obtained were compared to the standard curve values, and the AChE amounts (mU) were normalized to protein values (mU/ mg protein). The assessment was repeated three times in independent experiments blind to experimenter.

Measurement of $A\beta_{1-42}$ peptide in culture medium

The level of $A\beta_{1-42}$ peptide was measured according to a previous report [35] with minor modifications. Briefly, WT and PSEN1 E280A ChLNs were left in regular medium for 0, 2 and 4 days. Then, 100 µl of conditioned medium was collected, and the levels of secreted Aβ1-42 peptides were determined by a solid-phase sandwich ELISA (Invitrogen, Cat# KHB3544) following the manufacturer's instructions. The assessment was repeated three times in independent experiments blind to experimenter.

Intracellular calcium imaging

Intracellular calcium (Ca^{2+}) concentration changes evoked by cholinergic stimulation were assessed according to [36, 37] with minor modifications. For the measurement, the fluorescent dye Fluo-3 (Fluo-3 AM; Thermo Fisher Scientific, cat: F1242) was employed. The dye was dissolved in DMSO (1 mM) to form a stock solution. Before the experiments, the stock solution was diluted in neuronal buffer solution (NBS buffer: 137 mM NaCl, 5 mM KCl, 2.5 mM $CaCl_2$, 1 mM $MgCl_2$, pH 7.3, and 22 mM glucose). The working concentration of the dye was 2 µM. The WT and PSEN1 E280A ChLNs were incubated for 30 min at 37 °C with the dye-containing NBS and then washed five times. Intracellular Ca^{2+} transients were evoked by acetylcholine (1 mM final concentration) at 0, 2 and 4 days

bioRxiv preprint doi: https://doi.org/10.1101/735449; this version posted August 14, 2019. The copyright holder for this preprint (which was not certified by peer review) is the author/funder, who has granted bioRxiv a license to display the preprint in perpetuity. It is made available under aCC-BY 4.0 International license.

post differentiation. The measurements were carried out using the 400x objective of the microscope. Several regions of interest (ROIs) were defined in the visual field of the camera. One of the ROIs was cell-free, and the fluorescence intensity measured here was considered background fluorescence (F_{bg}). The time dependence of the fluorescence emission was acquired, and the fluorescence intensities (hence the Ca^{2+} levels) were represented by pseudocolors. To calculate the changes of the average Ca^{2+}-related fluorescence intensities, the F_{bg} value was determined from the cell-free ROI, and then the resting fluorescence intensities (F_{rest}) of the cell-containing ROIs were obtained as the average of the points recorded during a period of 10 s prior to the addition of acetylcholine. The peaks of the fluorescence transients were found by calculating the average of four consecutive points and identifying those points that gave the highest average value (F_{max}). The amplitudes of the Ca^{2+}-related fluorescence transients were expressed relative to the resting fluorescence ($\Delta F/F$) and were calculated by the following formula: $\Delta F/F=(F_{max}-F_{rest})/(F_{rest}-F_{bg})$. For the calculation of the fluorescence intensities, ImageJ was used. The terms fluorescence intensity was used as an indirect indicator of intracellular Ca^{2+} concentration. The assessment was repeated three times in independent experiments blind to experimenter.

JNK inhibition experiment

The ChLNs were left in regular medium for 0, 2 and 4 days alone or co-incubated with the anthrapyrazolone JNK inhibitor SP600125 (1 μM final concentration). This compound competes with ATP to inhibit the phosphorylation of c-JUN. After this time, cells were evaluated for p-TAU and t-TAU protein expression by immunofluorescence, as described above. The assessment was repeated three times in independent experiments blind to experimenter.

bioRxiv preprint doi: https://doi.org/10.1101/735449; this version posted August 14, 2019. The copyright holder for this preprint (which was not certified by peer review) is the author/funder, who has granted bioRxiv a license to display the preprint in perpetuity. It is made available under aCC-BY 4.0 International license.

Photomicrography and image analysis

Light microscopy photographs were taken using a Zeiss Axiostart 50 Fluorescence Microscope equipped with a Canon PowerShot G5 digital camera (Zeiss Wöhlk-Contact-Linsen, Gmb Schcönkirchen, Germany), and fluorescence microscopy photographs were taken using a Zeiss Axiostart 50 Fluorescence Microscope equipped with a Zeiss AxioCam Cm1 and (Zeiss Wöhlk-Contact-Linsfluoreen, Gmb Schcönkirchen, Germany) and Floyd Cells Imaging Station microscope. Fluorescence images were analyzed by ImageJ software (http://imagej.nih.gov/ij/). The figures were transformed into 8-bit images, and the background was subtracted. The cellular measurement regions of interest (ROIs) were drawn around the nucleus (for the case of transcription factors and apoptosis effectors) or over all cells (for cytoplasmic probes), and the fluorescence intensity was subsequently determined by applying the same threshold for cells in the control and treatment conditions. Mean fluorescence intensity (MFI) was obtained by normalizing total fluorescence to the number of nuclei.

Data analysis

In this experimental design, a vial of MSCs was thawed, cultured and the cell suspension was pipetted at a standardized cellular density of 2.6 x 10^4 cells/cm^2 into different wells of a 24-well plate. Cells (i.e., the biological and observational unit [38]) were randomized to wells by simple randomization (sampling without replacement method), and then wells (i.e., the experimental units) were randomized to treatments by similar method. Experiments were conducted in triplicate wells. The data from individual replicate wells were averaged to yield a value of n=1 for that experiment and this was repeated on three occasions blind to experimenter and/ or flow cytometer analyst for a final value of n=3

bioRxiv preprint doi: https://doi.org/10.1101/735449; this version posted August 14, 2019. The copyright holder for this preprint (which was not certified by peer review) is the author/funder, who has granted bioRxiv a license to display the preprint in perpetuity. It is made available under aCC-BY 4.0 International license.

[38]. Based on the assumptions that the experimental unit (i.e. the well) data comply with independence of observations, the dependent variable is normally distributed in each treatment group (Shapiro-Wilk test), and there is homogeneity of variances (Levene's test), the statistical significance was determined by a One-way analysis of variance (ANOVA) followed by Tukey's post hoc comparison calculated with GraphPad Prism 5.0 software. Differences between groups were only deemed significant when a p-value of < 0.05 (*), < 0.001 (**) and < 0.001 (***). All data are illustrated as the mean ± S.D.

bioRxiv preprint doi: https://doi.org/10.1101/735449; this version posted August 14, 2019. The copyright holder for this preprint (which was not certified by peer review) is the author/funder, who has granted bioRxiv a license to display the preprint in perpetuity. It is made available under aCC-BY 4.0 International license.

Results

PSEN1 E280A and wild-type WJ-MSCs show similar phenotypic, immunophenotypic, lineage differentiation and transdifferentiation

We first evaluated whether the PSEN1 E280A mutation affects the capacity of MSCs to generate mesodermal and ectodermal lineages through differentiation and transdifferentiation, respectively. Therefore, WJ-MSCs were isolated from ten umbilical cords of volunteers according to standard procedures [39], and PCR-RFLP electrophoretic profile analysis identified one umbilical cord sample out of ten as a carrier of the mutation *PSEN1* c.839A > C, p.E280A (PSEN1 E280A MSCs). Then, PSEN1 E280A MSCs and wild-type WJ-MSCs (WT PSEN1 MSCs) were further cultured and characterized for morphological, karyotype, immuno-phenotypic features and differentiation capabilities. As shown in **Figure 1,** WT PSEN1 and PSEN1 E280A MSCs displayed the typical colony-forming units (**Fig. 1A and 1B**), adherent growth, and fibroblast-like cellular morphology **(Fig. 1C and 1D)**. Karyotype analysis showed no chromosomal alterations (**Fig. 1E and 1F)**, and APOE genotyping analysis showed that PSEN1 E280A cells had the APOE*3/4 genotype and WT PSEN1 cells had the APOE*3/3 genotype. Flow cytometry analysis showed that both wild-type and mutant MSCs were positive (>95 % of positive cells) for mesenchymal associated markers CD73, CD90 and CD9 (**Fig. 1G and 1H)** but negative (<5 % of positive cells) for hematopoietic cell surface antigens CD34/ CD45. WT and PSEN1 E280A MSCs cultured in adipogenic, osteogenic, or chondrogenic induction medium differentiated into adipocytes (**Fig. 1J and 1P**), osteoblasts (**Fig. 1L and 1R**), and chondrocytes (**Fig. 1N and 1T)**, respectively, while MSCs cultured in regular culture medium were undifferentiated (**Fig. 1I, 1O, 1K, 1Q, 1M and 1S**).

bioRxiv preprint doi: https://doi.org/10.1101/735449; this version posted August 14, 2019. The copyright holder for this preprint (which was not certified by peer review) is the author/funder, who has granted bioRxiv a license to display the preprint in perpetuity. It is made available under aCC-BY 4.0 International license.

Additionally, MSCs were transdifferentiated into cholinergic-like neurons (ChLNs) from WJ-MSCs using a new method [25]. As shown in **Figure 2,** WT PSEN1 and PSEN1 E280A WJ-MSCs cultured in minimal culture medium (MCm) for 7 days expressed basal levels of protein MAP2 **(Fig. 2A and 2B)** and β Tub III **(Fig. 2A and 2C)** and undetectable levels of GFAP **(Fig. 2A and 2D)** and ChAT **(Fig. 2A and 2E)**. As expected, when the cells were exposed to cholinergic-N-Run medium (*Ch-N-Rm*) for 7 days [25], the levels of protein MAP2 **(Fig. 2A and B)**, β Tub III **(Fig. 2A and 2C)** and ChAT **(Fig. 2A and 2E)** were significantly higher than those in cells exposed to MCm. Noticeably, ChLNs remained negative for the specific glial cell lineage marker GFAP **(Fig. 2A and 2D)**. These observations were confirmed by immunofluorescence (**Fig. 2G-J).** Because the enzyme AChE catalyzes the breakdown of the neurotransmitter acetylcholine (ACh, [40], we evaluated whether ChLNs expressed a catalytically functional AChE enzyme. As shown in **Figure 2F**, the AChE enzyme presented basal activity in WJ-MSCs under MCm culture conditions (~8 ± 1.2 mU/mg protein), while the AChE enzyme activity was significantly higher (at least a 3-fold increase) in both control and mutant ChLNs (~26 ± 1.6 mU/mg protein). Remarkably, there was no significant difference in AChE enzymatic activity ($p < 0.05$) between WT and PSEN1 E280A ChLNs (at day 0 post differentiation).

bioRxiv preprint doi: https://doi.org/10.1101/735449; this version posted August 14, 2019. The copyright holder for this preprint (which was not certified by peer review) is the author/funder, who has granted bioRxiv a license to display the preprint in perpetuity. It is made available under aCC-BY 4.0 International license.

WT and PSEN1 E280A WJ-MSCs show similar levels of intracellular $A\beta_{42}$, oxidized DJ-1, mitochondrial membrane potential ($\Delta\Psi_m$) and reactive oxygen species (ROS)

Next, we evaluated whether the PSEN1 E280A mutation induced an overproduction of $A\beta_{42}$ and OS and alterations in $\Delta\Psi_m$ and ROS production in MSCs. Western blot measurements and immunofluorescence analysis revealed that both WT and PSEN1 E280A MSCs displayed undetectable levels of intracellular $A\beta_{42}$ and oxidized DJ-1 at days 0, 2 and 4 post differentiation **(Supplementary Fig. 1A-J).** Moreover, both WT and PSEN1 E280A MSCs displayed normal $\Delta\Psi_m$ (**Suppl. Fig. 2A),** undetectable levels of ROS (**Suppl. Fig. 2B)** and no changes in DNA content (**Suppl. Fig. 2C)** at days 0, 2 and 4 post differentiation according to flow cytometry (**Suppl. Fig. 2A-C)** and DCF/ MitoTracker fluorescence **(Suppl. Fig. 2D-K)**.

PSEN1 E280A cholinergic-like neurons (ChLNs) show high levels of intracellular $A\beta_{42}$, oxidized DJ-1, reactive oxygen species (ROS), loss of mitochondrial membrane potential ($\Delta\Psi_m$) and DNA fragmentation, but none of those markers are detected in WT PSEN1 ChLNs

The above observations prompted us to evaluate the same cell parameters in ChLNs. Therefore, WT PSEN1 and PSEN1 E280A ChLNs were left in regular culture medium until 0, 2 and 4 days post transdifferentiation. We initially verify that the $A\beta_{42}$ antibody (e.g., cat# AB5078P, Sigma-Aldrich) recognize monomers as well as oligomers of $A\beta_{42}$. Effectively, the $A\beta_{42}$ antibody was capable to recognize the "unaggregated" (monomers) and large oligomeric forms of synthetic $A\beta_{42}$ peptide (**Fig. 3A).** Western blot revealed that WT PSEN1 ChLNs displayed low or undetectable levels of intracellular $A\beta_{42}$ oligomers

bioRxiv preprint doi: https://doi.org/10.1101/735449; this version posted August 14, 2019. The copyright holder for this preprint (which was not certified by peer review) is the author/funder, who has granted bioRxiv a license to display the preprint in perpetuity. It is made available under aCC-BY 4.0 International license.

(**Fig. 3A and 3B)** and oxidized DJ-1 **(Fig. 3A and 3C)**, whereas flow cytometry showed no loss of $\Delta\Psi_m$ (**Fig. 4A-C)** and no ROS generation (**Fig. 4D-F)** at any time tested. However, PSEN1 E280A ChLNs exhibited significantly higher levels of intracellular $A\beta_{42}$ oligomers **(Fig. 3A and 3B)** and oxidized DJ-1 **(Fig. 3A and 3C)** and lower $\Delta\Psi_m$ than WT PSEN1 ChLNs at days 2 and 4 (**Fig. 4B and 4C)**. These observations were confirmed by immunofluorescence microscopy (**Fig. 3D-K, and Fig. 4J'-O')**. Interestingly, PSEN1 E280A ChLNs showed high levels of ROS production as early as day 0 (**Fig. 4D, M'' and Q)** and at day 2 (**Fig. 4E, N'' and Q),** but ROS were severely reduced at day 4 (**Fig. 4F, O'' and Q)**. Furthermore, both WT and PSEN1 E280A ChLNs exhibited a typical quiescent cell cycle (i.e., phase G_0, **Fig. 4G-I**) and showed similar numbers of cells in the $SubG_0$ population at day 0 **(Fig. 4G)**; nonetheless, the $SubG_0$ population was significantly elevated in PSEN1 E280A ChLNs at day 2 **(**~15% compared to that in WT cells; **Fig. 4H)** and day 4 **(**~12% compared to WT cells; **Fig. 4I)** according to propidium iodide (PI) fluorescence analysis.

PSEN1 E280A ChLNs display activation of p53, PUMA, c-JUN and CASPASE-3

Aβ-induced OS is linked to apoptosis, a regulated type of cell death, by triggering a signaling death cascade involving transcription factors, kinases, pro-apoptotic proteins and proteases [41, 42]. Therefore, we used the transcription factors p53 and c-JUN, pro-apoptotic BH3-only protein PUMA, and protease CASPASE-3 as cell death markers to examine the pro-death activity of $A\beta_{42}$ in ChLNs over time. As shown in **Figure 5**, while WT PSEN1 ChLNs showed no detectable levels of apoptogenic proteins at any time tested (**Fig. 5A-E)**, the PSEN1 E280A ChLNs displayed significant detection of c-JUN (at day 0,

bioRxiv preprint doi: https://doi.org/10.1101/735449; this version posted August 14, 2019. The copyright holder for this preprint (which was not certified by peer review) is the author/funder, who has granted bioRxiv a license to display the preprint in perpetuity. It is made available under aCC-BY 4.0 International license.

2 and 4, **Fig. 5A and 5B**), p53 (at day 2 and 4, **Fig. 5A and 5C**), PUMA (at day 4, **Fig. 5A and 5D**) and CASP-3 (at day 4, **Fig. 5A and 5E)**. These observations were confirmed by immunofluorescence analysis at day 2 (**data not shown**) and day 4 (**Fig. 5F-M**).

PSEN1 E280A ChLNs show reduced functional response to acetylcholine (ACh), low acetylcholinesterase activity, and generation of high levels of extracellular $A\beta_{42}$ peptide

We further investigated whether WT and PSEN1 E280A ChLNs responded to ACh stimuli as an evaluation of cholinergic neuronal Ca^{2+} responsiveness and functionality [25]. To this aim, we simultaneously measured the secreted levels of $A\beta_{42}$ and evaluated the response of ChLNs to ACh. ELISA revealed that both WT PSEN1 and PSEN1 E280A ChLNs secreted similarly low levels of extracellular $A\beta_{42}$ at days 0 and 2, but at day 4, PSEN1 E280A ChLNs showed significantly higher extracellular levels of $A\beta_{42}$ compared to PSEN1 WT ChLNs **(**~3.2-f.i., **Fig. 6A)**. For functional analysis, both control and mutant PSEN1 ChLN cultures were puffed with ACh (1 mM final concentration) into a bath solution. As expected, ACh induced a transient elevation of intracellular Ca^{2+} in WT PSEN1 ChLNs at day 0 **(Fig. 6B, 6D)**, 2 **(Fig. 6E, 6G)** and 4 **(Fig. 6H, 6J)**. The average fluorescence change ($\Delta F/F$) was 6.4 ± 0.6, 6.4 ± 0.7 and 5.9 ± 1.4–fold, respectively, with a mean duration of 40 ± 10 s ($n = 20$ ChLN cells imaged, $N = 3$ dishes) according to cytoplasmic Ca^{2+} responses to Fluo-3-mediated imaging. Interestingly, PSEN1 E280A ChLNs showed higher intracellular Ca^{2+} in response to ACh treatment at day 0 **(Fig. 6C and 6D)** and 2 **(Fig. 6F and 6G)** than WT PSEN1 ChLNs (**Fig. 6D and 6G)**. The average fluorescence change ($\Delta F/ F$) was 4.6 ± 1.2 and 5.1 ± 1.1–fold, respectively, with a mean duration of 40 ± 10 s

bioRxiv preprint doi: https://doi.org/10.1101/735449; this version posted August 14, 2019. The copyright holder for this preprint (which was not certified by peer review) is the author/funder, who has granted bioRxiv a license to display the preprint in perpetuity. It is made available under aCC-BY 4.0 International license.

(*n = 30* ChLN cells imaged, *N = 3* dishes). Nevertheless, we found a significant difference in the ΔF/ F response (ΔF/ F = 1.1 ± 0.75, $p < 0.001$) in PSEN1 E280A ChLNs exposed to ACh at 4 days post differentiation **(Fig. 6I and 6J)** compared to that in WT ChLNs (**Fig. 6H and 6J)**.

The above findings compelled us to evaluate whether ChLNs expressed a catalytically functional acetylcholinesterase (AChE) enzyme at similar times post differentiation. As shown in **Figure 6K**, the AChE enzyme showed similar catalytic activity at days 2 and 4 in both WT PSEN1 and PSEN1 E280A ChLNs. However, the AChE enzyme activity in PSEN1 E280A ChLNs was significantly lower (at least 5-fold) than that in WT PSEN1 ChLNs at day 4.

PSEN1 E280A ChLNs induce phosphorylation of TAU protein

Several experimental data support Aβ-induced TAU pathology (e.g., [43]). We thus evaluated whether PSEN1 E280A ChLNs display abnormal levels of phosphorylated TAU protein at residues Ser^{202} and Thr^{205}, two well-known hyperphosphorylated epitopes involved in AD pathology [44]. To this end, wild-type and mutant ChLNs were left in regular culture medium for 0, 2 and 4 days. Then, the ratio of phosphorylated TAU (p-TAU)/total TAU (t-TAU) was determined by western blot and immunofluorescence imaging analyses. As shown in **Figure 7**, while WT PSEN1 ChLNs showed no phosphorylation of TAU protein according to western blot **(Fig. 7A-B)** and immunofluorescence microscopy **(Fig. 7C'-E'** and **7I)**, PSEN1 E280A ChLNs presented an increase in the p-TAU/ t-TAU ratio at 4 days post transdifferentiation (**Fig. 7A-B; 7F'-H'**

bioRxiv preprint doi: https://doi.org/10.1101/735449; this version posted August 14, 2019. The copyright holder for this preprint (which was not certified by peer review) is the author/funder, who has granted bioRxiv a license to display the preprint in perpetuity. It is made available under aCC-BY 4.0 International license.

and **7I)**. JNK has been suggested to phosphorylate TAU at the Ser202/Thr205 epitopes [45]. Therefore, we determined whether JNK was implicated in TAU phosphorylation in ChLNs. To this end, PSEN1 E280A ChLNs were incubated with the JNK inhibitor SP600125 for 0, 2 and 4 days. Notably, the p-TAU/ t-TAU ratio remained unaltered at 0 **(Fig. 7J-K, 7O' and 7R)**, 2 **(Fig. 7J-K, 7P' and 7R)** and 4 days post differentiation **(Fig. 7J-K, 7Q' and 7R)**.

bioRxiv preprint doi: https://doi.org/10.1101/735449; this version posted August 14, 2019. The copyright holder for this preprint (which was not certified by peer review) is the author/funder, who has granted bioRxiv a license to display the preprint in perpetuity. It is made available under aCC-BY 4.0 International license.

Discussion

Currently, the neuropathology of AD includes extracellular deposits of Aβ in plaques, intracellular neurofibrillary tangles comprising hyperphosphorylated TAU, synaptic dysfunction, and neuronal death. In an effort to explain such observations, several theories have been proposed [46]; however, the amyloid cascade hypothesis has prevailed for more than 25 years [47]. The Aβ hypothesis postulates that an imbalance in the production of extracellular $A\beta_{42}$ plaques by mutations in at least three genes (e.g., *APP, PSEN1; PSEN2*) is an early initiating factor in AD. However, experimental therapies targeting Aβ have thus far been unsuccessful [48]. Several factors have probably contributed to the failures in AD drug development, including unsuitable preclinical research models that do not fully recapitulate the human disease; consequently, druggable targets remain missing [49]. Furthermore, the mechanism(s) by which $A\beta_{42}$ might induce toxicity is not yet fully established. Because UC-MSCs possess plasticity properties enabling them to transdifferentiate into non-mesenchymal lineages, they provide a unique opportunity to study the effect of *PSEN1* mutations in neuronal cells. Most importantly, MSC-derived neurons are natural, genetically modified models of the FAD PSEN1 mutation. Here, we used UC-MSCs bearing the mutation PSEN1 E280A for the first time and found that the mutation alters none of the typical MSC characteristics, such as colony-forming capacity, fibroblast-like morphology, immunophenotype and/or ability to differentiate or transdifferentiate into ChLNs. Furthermore, we did not detect any $A\beta_{42}$ produced by the cells or any other cellular alterations (e.g., ROS production, mitochondria depolarization, and oxidation of stress sensor DJ-1) in mutant MSCs. These observations suggest that the

bioRxiv preprint doi: https://doi.org/10.1101/735449; this version posted August 14, 2019. The copyright holder for this preprint (which was not certified by peer review) is the author/funder, who has granted bioRxiv a license to display the preprint in perpetuity. It is made available under aCC-BY 4.0 International license.

PSEN1 E280A mutation might not affect the physiology of the multipotent MS cells at this stage of development.

In this study, we report for the first time that ChLNs derived from hMSCs carrying the PSEN1 E280A mutation recapitulate typical pathologic features of AD at 4 days post transdifferentiation, including increased secretion of $A\beta_{42}$, intracellular accumulation of $A\beta_{42}$, and TAU phosphorylation. Furthermore, PSEN1 E280A ChLNs not only show OS and apoptosis markers but also display Ca^{2+} flux dysregulation and altered acetylcholinesterase activity. Our data provide evidence that intracellular Aβ peptide specifically induces neurotoxicity through a temporal and sequential order of molecular events in PSEN1 E280A ChLNs. We found intracellular $A\beta_{42}$ accumulation in ChLNs as early day zero (day 0) after 7 days transdifferentiation, at which time fully developed ChLNs were obtained [25]. Whether intracellular $A\beta_{42}$ builds up because a portion of the generated $A\beta_{42}$ is not secreted and consequently remains intracellular or whether secreted $A\beta_{42}$ is taken up by the cell to form these intracellular pools requires further investigation. However, recent data support the former view. Indeed, the PSEN1 L166P and G384A mutations have been demonstrated to cause relocalization of γ-secretase, which significantly promotes the generation of intracellular long $A\beta_{42}$ [50]. Although whether the PSEN1 E280A mutation induces relocalization of γ-secretase, similar to PSEN1 mutations, is not known, our data suggest that the PSEN1 E280A mutation strongly enhances intraneuronal $A\beta_{42}$ in ChLNs. Taken together, these results support the view that intracellular accumulation of $A\beta_{42}$ is the earliest event in the development of the neuropathological changes of AD [51]. Interestingly, we simultaneously found a significant

bioRxiv preprint doi: https://doi.org/10.1101/735449; this version posted August 14, 2019. The copyright holder for this preprint (which was not certified by peer review) is the author/funder, who has granted bioRxiv a license to display the preprint in perpetuity. It is made available under aCC-BY 4.0 International license.

increase in DCF fluorescent-positive cells, DJ-1 Cys^{106}–sulfonate (DJ-1 $Cys^{106}SO_3$), which is the most sensitive thiol group towards H_2O_2 reactivity [52], and activation of transcription factor c-JUN in PSEN1 E280A ChLNs. These observations suggest that $A\beta_{42}$ (oligomers) > H_2O_2 > oxDJ-1Cys^{106}-SO_3 and c-JUN are the earliest events detectable in PSEN1 E280A ChLNs. These findings imply that $A\beta_{42}$ can trigger events related to oxidative stress and cell death [53]. How then does intracellular $A\beta_{42}$ generate H_2O_2? Several mechanisms for the toxicity of $A\beta_{42}$ have been suggested, including free radical transfer reactions via oxidation of the sulfur atom of methionine residue 35 in $A\beta_{42}$ to reduce dioxygen (O_2) into anion superoxide radical ($O_2^{\cdot-}$), which in turn dismutates to H_2O_2; the catalyzation of the formation and production of ROS (e.g., H_2O_2) by Aβ– metal (e.g., Cu^{2+}, Cu^{1+}, Fe^{2+}) complexes [54]; and targeting of mitochondria [55]. Whatever the mechanism, we demonstrated for the first time that $A\beta_{42}$ endogenously produces H_2O_2 in PSEN1 E280A ChLNs. Because H_2O_2 can function as a second messenger [56], it might also activate other redox proteins, such as apoptosis-signal regulating kinase 1 (ASK-1, [57], which in turn directly or indirectly activate other signaling pathways, e.g., JNK/c-JUN [58]. We found that $A\beta_{42}$ induced phosphorylation of c-JUN [59], p53 and PUMA in PSEN1 E280A ChLNs. Notably, c-JUN- and p53-dependent apoptosis is triggered by transactivation of the pro-apoptotic gene PUMA [60-62]. Remarkably, JNK can also stabilize and activate p53 [63]. Taken together, these results suggest that $A\beta_{42}$ > H_2O_2 activates a cascade of events leading to the JNK> c-JUN, p53 > PUMA pathway. Although PUMA has been shown to cooperate with direct activator proteins (e.g., BAX) to promote mitochondrial outer membrane permeabilization (MOMP) and apoptosis [64], the exact mechanism by which MOMP occurs is not fully understood [65]. Interestingly, PSEN1

bioRxiv preprint doi: https://doi.org/10.1101/735449; this version posted August 14, 2019. The copyright holder for this preprint (which was not certified by peer review) is the author/funder, who has granted bioRxiv a license to display the preprint in perpetuity. It is made available under aCC-BY 4.0 International license.

E280A ChLNs showed loss of $\Delta\Psi_m$ concomitant with overexpression of CASPASE-3 and fragmentation of nuclei at day 4 post transdifferentiation. These observations suggest that mitochondria play an important role in intracellular $A\beta_{42}$-induced apoptosis in mutant ChLNs. However, whether $\Delta\Psi_m$ dysfunction is a consequence of a direct effect of intracellular $A\beta_{42}$ on the organelle [55, 66] or whether the damage is the result of the impact of PUMA on mitochondria is an unresolved issue. Our findings suggest that both $A\beta_{42}$ / PUMA might separately or jointly damage $\Delta\Psi_m$. Taken together, these data indicate that $A\beta_{42}$ induces a cascade of events in PSEN1 E280A ChLNs through the H_2O_2 signaling pathway involving CASP-3, as an end executer protein, and DNA fragmentation of nuclei, all indicative of apoptosis. Taken together, these data comply with the idea that intraneuronal accumulation of the $A\beta_{42}$ peptide is the first step of a lethal cascade in FAD neurons [67].

Neuronal calcium (Ca^{2+}) dyshomeostasis has been proposed to play a crucial role in AD disease progression [68]. However, the mechanisms of Ca^{2+} dysregulation are not clear. In contrast to Demuro and Parker [69], who found that intracellular $A\beta_{42}$ oligomers disrupted cellular Ca^{2+} regulation, we observed no Ca^{2+} dysregulation in PSEN1 E280A ChLNs evaluated at 0, 2, and 4 days post transdifferentiation. This discrepancy can be explained by differences in experimental methodology. Whereas those authors elucidated the actions of intracellular $A\beta_{42}$ by imaging Ca^{2+} responses to injections of $A\beta_{42}$ oligomers into *Xenopus* oocytes, we directly imaged Ca^{2+} responses to endogenously generated intracellular $A\beta_{42}$ in mutant ChLNs. Under the present experimental conditions, we concluded that intracellular $A\beta_{42}$ did not affect Ca^{2+} flux in PSEN1 E280A ChLNs. Increasing evidence has shown that

bioRxiv preprint doi: https://doi.org/10.1101/735449; this version posted August 14, 2019. The copyright holder for this preprint (which was not certified by peer review) is the author/funder, who has granted bioRxiv a license to display the preprint in perpetuity. It is made available under aCC-BY 4.0 International license.

extracellular Aβ specifically interacts with nAChRs, resulting in Ca^{2+} dysregulation [70]. We found that the PSEN1 E280A ChLN response to ACh was significantly reduced by day 4 post transdifferentiation. Notably, Aβ has been shown to directly affect α7 nicotinic ACh receptor (α7 nAChR) function by acting as an agonist (~100 nM) and a negative modulator (at high concentrations) [71]. Consistent with this view, we confirmed that PSEN1 E280A ChLNs secreted aberrant amounts of $Aβ_{42}$ (e.g., ~2500-f.i.) compared to WT PSEN1 ChLNs. These observations confirm that overproduction of extracellular $Aβ_{42}$ is a paramount feature of the majority of PSEN1 mutations *in vitro* and *in vivo* [5], including the E280A mutation [21]. Despite these observations, further investigation is required to determine whether α7 nAChRs specifically are affected by $Aβ_{42}$ in PSEN1 E280A ChLNs. In contrast to others (e.g., [72]), our observations do not support the common view that extracellular Aβ is capable of increasing neuronal Ca^{2+} flux through $Aβ_{42}$-forming pores. However, we do not discard the possibility that given a longer incubation time, $Aβ_{42}$ could affect Ca^{2+} flux via $Aβ_{42}$-forming pores in PSEN1 E280A ChLNs. Taken together, and our data suggest that extracellular $Aβ_{42}$ might bind to nAChRs in PSEN1 E280A ChLNs, affecting neuronal Ca^{2+} flux.

The accumulation of hyperphosphorylated TAU in neurons leads to neurofibrillary degeneration in AD [73]. Mounting evidence suggests that TAU pathogenesis is promoted by $Aβ_{42}$ [74, 75]. In line with this, we found that PSEN1 E280A ChLNs showed hyperphosphorylation of TAU protein. In fact, PSEN1 E280A ChLNs exhibited a significantly higher p-TAU/ t-TAU ratio than WT PSEN1 ChLNs at 4 days post transdifferentiation. These observations imply that $Aβ_{42}$ signaling precedes TAU

bioRxiv preprint doi: https://doi.org/10.1101/735449; this version posted August 14, 2019. The copyright holder for this preprint (which was not certified by peer review) is the author/funder, who has granted bioRxiv a license to display the preprint in perpetuity. It is made available under aCC-BY 4.0 International license.

phosphorylation [75, 76]. Moreover, these findings comply with the notion that $A\beta_{42}$ accumulation affects TAU pathology [77]. However, the molecular link between Aβ and TAU is still not yet completely defined. In agreement with others [78], our data suggest that JNK is a strong candidate TAU kinase involved in the hyperphosphorylation of TAU in PSEN1 E280A ChLNs. This assumption is supported by two observations. First, JNK phosphorylates TAU at Ser^{202}/ Thr^{205} [45], two phosphorylation epitopes identified in the present study. Second, PSEN1 E280A ChLNs exposed to the JNK inhibitor SP600125 significantly reduced TAU phosphorylation. Given that JNK plays a pivotal role in both OS-induced apoptosis and TAU phosphorylation, these findings identify JNK as a potential therapeutic target [79]. Although we do not discard the possibility that other kinases might be implicated in TAU pathology (e.g., LRRK2, GSK-3, Cdk5) , our findings suggest that JNK plays a key role in TAU hyperphosphorylation in PSEN1 E280A ChLNs. Outstandingly, MSC-derived ChLNs not only replicate the pathophysiology of AD, i.e., intracellular accumulation of $A\beta_{42}$ and TAU phosphorylation as similarly reported in the PSEN1 iPSC model [19, 20], but also replicate the intracellular aggregation of $A\beta_{42}$ and OS phenotypes in AD model iPSCs [18, 80]. Therefore, MSC-derived PSEN1 neurons should be considered equivalent to iPSC-derived PSEN1 neurons. Moreover, our results suggest that PSEN1 E280A-induced neural alterations may precede $A\beta_{42}$ deposition and that those alterations represent longstanding effects of intracellular $A\beta_{42}$ oligomeric toxicity and possibly even developmental changes. The molecular alterations might start when neurons develop into neuron-specific cholinergic-type cells or may even exist at birth. These findings may explain why functional and structural brain changes manifest in children (9-17 years old) and young individuals (18-26 years) who are carriers of the

bioRxiv preprint doi: https://doi.org/10.1101/735449; this version posted August 14, 2019. The copyright holder for this preprint (which was not certified by peer review) is the author/funder, who has granted bioRxiv a license to display the preprint in perpetuity. It is made available under aCC-BY 4.0 International license.

PSEN1 E280A mutation [81, 82]. Furthermore, these observations suggest that intracellular $A\beta_{42}$ oligomeric toxicity is an early and slowly progressive process that might damage neuronal cells in a TAU-dependent and independent fashion (OS, $\Delta\Psi_m$ shutdown, apoptosis and intraneuronal Ca^{2+} dysregulation) more than two decades before the stage of dementia [6, 83].

Conclusion

We demonstrate that intracellular accumulation of $A\beta_{42}$, generation of H_2O_2, oxidation of the DJ-1 protein (DJ-1 Cys^{106}-SO_3), and activation of the pro-apoptosis protein c-JUN were the earliest cellular changes in PSEN1 E280A ChLNs (day 0, **Fig. 8 step 1, s2, s3**, **s4/s5)**. These changes were followed by the activation of pro-apoptosis proteins p53 (**s6)** and PUMA (**s7**), loss of mitochondria membrane potential ($\Delta\Psi_m$, **s8),** activation of CASP-3 (**s9),** fragmentation of nuclei (**s10),** and complete expression of markers of apoptosis (at day 4). These biochemical abnormalities were found concomitant with irregular secretion of $A\beta_{42}$ (day 4, **s11**), Ca^{2+} flux dysregulation (**s12)**, diminished secretion of AChE (**s13**), and hyperphosphorylation of TAU protein (day 4, **s14**). Therefore, our data support the view that FAD PSEN1 E280A cholinergic neuronal pathology is instigated by soluble, early intracellular accumulation of $A\beta_{42}$ oligomers [84, 85]. These findings raise the question of whether strategies to remove extracellular $A\beta_{42}$ such as immunotherapy [86] should be complemented with treatments to remove intracellular $A\beta_{42}$ and OS (i.e., H_2O_2) to avoid apoptosis and TAU pathology and treatment with nAChR agonists to increase neuronal functionality. The present findings naturally (i.e., not genetically manipulated) recapitulated for the first time the neuropathological features of FAD PSEN1 E280A. We anticipate that

bioRxiv preprint doi: https://doi.org/10.1101/735449; this version posted August 14, 2019. The copyright holder for this preprint (which was not certified by peer review) is the author/funder, who has granted bioRxiv a license to display the preprint in perpetuity. It is made available under aCC-BY 4.0 International license.

the present *in vitro* model will inspire new and innovative therapies for early onset PSEN1 E280A patients.

bioRxiv preprint doi: https://doi.org/10.1101/735449; this version posted August 14, 2019. The copyright holder for this preprint (which was not certified by peer review) is the author/funder, who has granted bioRxiv a license to display the preprint in perpetuity. It is made available under aCC-BY 4.0 International license.

Acknowledgments: We greatly acknowledge KA Herrera-Galeano (Nurse), F Piedrahita (Nurse), L Lopez (Psychologist) and AA Espinosa-Rojas (MD) for technical support for obtaining human umbilical cord tissue at Hospital San Juan de Dios, Yarumal, Colombia. We specially acknowledge the newborns' parents for human umbilical cord tissue. Compliance with Ethical Standards

Funding: This study was funded by Colciencias grant # 1115-807-**62912**, contract #749-2018 to MJ-Del-Rio and CV-P. MM-P is enrolled as a post-Doctoral fellowship grant # 784-2017 from Colciencias.

Conflict of interest: The authors have declared that no competing interests exist.

Ethical Approval: All procedures performed in studies involving human participants were in accordance with the ethical standards of the Ethics Committee for Research Act #13-2015 from Fundacion Hospitalaria San Vicente de Paul and with the 1964 Helsinki declaration and its later amendments or comparable ethical standards.

Informed consent: Informed consent was obtained from all parents of newborns' human umbilical cords (hUCs) collected in the study.

Author Contributions

CV-P and MJ-Rio designed and conceived the in vitro experiments; VS-M and MM-P performed in vitro experiments. FL contributed with clinical profile of FAD UC donations and genotype profile; MJ-Del-Rio and CV-P wrote the original draft. The authors analyzed data, reviewed, edited and approved the final version of the paper.

bioRxiv preprint doi: https://doi.org/10.1101/735449; this version posted August 14, 2019. The copyright holder for this preprint (which was not certified by peer review) is the author/funder, who has granted bioRxiv a license to display the preprint in perpetuity. It is made available under aCC-BY 4.0 International license.

References

1. Lane CA, Hardy J, Schott JM. Alzheimer's disease. Eur J Neurol. 2018;25(1):59-70. Epub 2017/09/06. doi: 10.1111/ene.13439. PubMed PMID: 28872215.
2. Douchamps V, Mathis C. A second wind for the cholinergic system in Alzheimer's therapy. Behav Pharmacol. 2017;28(2 and 3-Spec Issue):112-23. Epub 2017/02/28. doi: 10.1097/fbp.0000000000000300. PubMed PMID: 28240674.
3. Perl DP. Neuropathology of Alzheimer's disease. Mt Sinai J Med. 2010;77(1):32-42. Epub 2010/01/27. doi: 10.1002/msj.20157. PubMed PMID: 20101720; PubMed Central PMCID: PMCPMC2918894.
4. Steiner H, Fukumori A, Tagami S, Okochi M. Making the final cut: pathogenic amyloid-β peptide generation by γ-secretase. Cell Stress. 2018;2(11):292-310. doi: 10.15698/cst2018.11.162.
5. Sun L, Zhou R, Yang G, Shi Y. Analysis of 138 pathogenic mutations in presenilin-1 on the in vitro production of Abeta42 and Abeta40 peptides by gamma-secretase. Proc Natl Acad Sci U S A. 2017;114(4):E476-e85. Epub 2016/12/09. doi: 10.1073/pnas.1618657114. PubMed PMID: 27930341; PubMed Central PMCID: PMCPMC5278480.
6. Acosta-Baena N, Sepulveda-Falla D, Lopera-Gómez CM, Jaramillo-Elorza MC, Moreno S, Aguirre-Acevedo DC, et al. Pre-dementia clinical stages in presenilin 1 E280A familial early-onset Alzheimer's disease: a retrospective cohort study. Lancet Neurol. 2011;10(3):213-20. doi: 10.1016/S1474-4422(10)70323-9. PubMed PMID: 21296022.
7. Lopera F, Ardilla A, Martinez A, Madrigal L, Arango-Viana JC, Lemere CA, et al. Clinical features of early-onset Alzheimer disease in a large kindred with an E280A presenilin-1 mutation. Jama. 1997;277(10):793-9. Epub 1997/03/12. PubMed PMID: 9052708.
8. Sepulveda-Falla D, Glatzel M, Lopera F. Phenotypic profile of early-onset familial Alzheimer's disease caused by presenilin-1 E280A mutation. J Alzheimers Dis. 2012;32(1):1-12. doi: 10.3233/JAD-2012-120907. PubMed PMID: 22766738.
9. Fuller JT, Cronin-Golomb A, Gatchel JR, Norton DJ, Guzman-Velez E, Jacobs HIL, et al. Biological and Cognitive Markers of Presenilin1 E280A Autosomal Dominant Alzheimer's Disease: A Comprehensive Review of the Colombian Kindred. J Prev Alzheimers Dis. 2019;6(2):112-20. Epub 2019/02/14. doi: 10.14283/jpad.2019.6. PubMed PMID: 30756118.
10. Lalli MA, Cox HC, Arcila ML, Cadavid L, Moreno S, Garcia G, et al. Origin of the PSEN1 E280A mutation causing early-onset Alzheimer's disease. Alzheimers Dement. 2014;10(5 Suppl):S277-S83.e10. Epub 2013/11/19. doi: 10.1016/j.jalz.2013.09.005. PubMed PMID: 24239249; PubMed Central PMCID: PMCPMC4019728.
11. Heilig EA, Gutti U, Tai T, Shen J, Kelleher RJ, 3rd. Trans-dominant negative effects of pathogenic PSEN1 mutations on gamma-secretase activity and Abeta production. J Neurosci. 2013;33(28):11606-17. Epub 2013/07/12. doi: 10.1523/jneurosci.0954-13.2013. PubMed PMID: 23843529; PubMed Central PMCID: PMCPMC3724549.
12. Zhou R, Yang G, Shi Y. Dominant negative effect of the loss-of-function gamma-secretase mutants on the wild-type enzyme through heterooligomerization. Proc Natl Acad Sci U S A. 2017;114(48):12731-6. Epub 2017/10/29. doi: 10.1073/pnas.1713605114. PubMed PMID: 29078389; PubMed Central PMCID: PMCPMC5715776.
13. Lemere CA, Lopera F, Kosik KS, Lendon CL, Ossa J, Saido TC, et al. The E280A presenilin 1 Alzheimer mutation produces increased A beta 42 deposition and severe cerebellar pathology. Nat Med. 1996;2(10):1146-50. PubMed PMID: 8837617.
14. Velez-Pardo C, Arellano JI, Cardona-Gomez P, Jimenez Del Rio M, Lopera F, De Felipe J. CA1 hippocampal neuronal loss in familial Alzheimer's disease presenilin-1 E280A mutation is related to epilepsy. Epilepsia. 2004;45(7):751-6. Epub 2004/07/03. doi: 10.1111/j.0013-9580.2004.55403.x. PubMed PMID: 15230697.
15. Fleisher AS, Chen K, Quiroz YT, Jakimovich LJ, Gomez MG, Langois CM, et al. Florbetapir PET analysis of amyloid-β deposition in the presenilin 1 E280A autosomal dominant

bioRxiv preprint doi: https://doi.org/10.1101/735449; this version posted August 14, 2019. The copyright holder for this preprint (which was not certified by peer review) is the author/funder, who has granted bioRxiv a license to display the preprint in perpetuity. It is made available under aCC-BY 4.0 International license.

Alzheimer's disease kindred: a cross-sectional study. Lancet Neurol. 2012;11(12):1057-65. doi: 10.1016/S1474-4422(12)70227-2. PubMed PMID: 23137949; PubMed Central PMCID: PMCPMC3515078.

16. Quiroz YT, Sperling RA, Norton DJ, Baena A, Arboleda-Velasquez JF, Cosio D, et al. Association Between Amyloid and Tau Accumulation in Young Adults With Autosomal Dominant Alzheimer Disease. JAMA Neurol. 2018;75(5):548-56. Epub 2018/02/13. doi: 10.1001/jamaneurol.2017.4907. PubMed PMID: 29435558; PubMed Central PMCID: PMCPMC5885174.

17. Kumar K, Kumar A, Keegan RM, Deshmukh R. Recent advances in the neurobiology and neuropharmacology of Alzheimer's disease. Biomed Pharmacother. 2018;98:297-307. Epub 2017/12/24. doi: 10.1016/j.biopha.2017.12.053. PubMed PMID: 29274586.

18. Oksanen M, Petersen AJ, Naumenko N, Puttonen K, Lehtonen S, Gubert Olive M, et al. PSEN1 Mutant iPSC-Derived Model Reveals Severe Astrocyte Pathology in Alzheimer's Disease. Stem Cell Reports. 2017;9(6):1885-97. Epub 2017/11/21. doi: 10.1016/j.stemcr.2017.10.016. PubMed PMID: 29153989; PubMed Central PMCID: PMCPMC5785689.

19. Ochalek A, Mihalik B, Avci HX, Chandrasekaran A, Teglasi A, Bock I, et al. Neurons derived from sporadic Alzheimer's disease iPSCs reveal elevated TAU hyperphosphorylation, increased amyloid levels, and GSK3B activation. Alzheimers Res Ther. 2017;9(1):90. Epub 2017/12/02. doi: 10.1186/s13195-017-0317-z. PubMed PMID: 29191219; PubMed Central PMCID: PMCPMC5709977.

20. Yang J, Zhao H, Ma Y, Shi G, Song J, Tang Y, et al. Early pathogenic event of Alzheimer's disease documented in iPSCs from patients with PSEN1 mutations. Oncotarget. 2017;8(5):7900-13. Epub 2016/12/08. doi: 10.18632/oncotarget.13776. PubMed PMID: 27926491; PubMed Central PMCID: PMCPMC5352369.

21. Mendivil-Perez M, Velez-Pardo C, Kosik KS, Lopera F, Jimenez-Del-Rio M. iPSCs-derived nerve-like cells from familial Alzheimer's disease PSEN 1 E280A reveal increased amyloid-beta levels and loss of the Y chromosome. Neurosci Lett. 2019;703:111-8. Epub 2019/03/25. doi: 10.1016/j.neulet.2019.03.032. PubMed PMID: 30904577.

22. Cheng H, Ghetu N, Wallace C, Wei F, Liao S. The Impact of Mesenchymal Stem Cell Source on Proliferation, Differentiation, Immunomodulation and Therapeutic Efficacy. J Stem Cell Res Ther. 2014;4(10):1-8. doi: 10.4172/2157-7633.1000237.

23. Zhang HT, Fan J, Cai YQ, Zhao SJ, Xue S, Lin JH, et al. Human Wharton's jelly cells can be induced to differentiate into growth factor-secreting oligodendrocyte progenitor-like cells. Differentiation. 2010;79(1):15-20. Epub 2009/10/06. doi: 10.1016/j.diff.2009.09.002. PubMed PMID: 19800163.

24. Bonilla-Porras AR, Velez-Pardo C, Jimenez-Del-Rio M. Fast transdifferentiation of human Wharton's jelly mesenchymal stem cells into neurospheres and nerve-like cells. J Neurosci Methods. 2017;282:52-60. Epub 2017/03/14. doi: 10.1016/j.jneumeth.2017.03.005. PubMed PMID: 28286110.

25. Mendivil-Perez M, Velez-Pardo C, Jimenez-Del-Rio M. Direct transdifferentiation of human Wharton's jelly mesenchymal stromal cells into cholinergic-like neurons. J Neurosci Methods. 2019;312:126-38. Epub 2018/11/26. doi: 10.1016/j.jneumeth.2018.11.019. PubMed PMID: 30472070.

26. Choi J, Lee S, Mallard W, Clement K, Tagliazucchi GM, Lim H, et al. A comparison of genetically matched cell lines reveals the equivalence of human iPSCs and ESCs. Nat Biotechnol. 2015;33(11):1173-81. Epub 2015/10/27. doi: 10.1038/nbt.3388. PubMed PMID: 26501951; PubMed Central PMCID: PMCPMC4847940.

27. Song L, Tsai AC, Yuan X, Bejoy J, Sart S, Ma T, et al. Neural Differentiation of Spheroids Derived from Human Induced Pluripotent Stem Cells-Mesenchymal Stem Cells Coculture. Tissue Eng Part A. 2018;24(11-12):915-29. Epub 2017/11/22. doi: 10.1089/ten.TEA.2017.0403. PubMed PMID: 29160172; PubMed Central PMCID: PMCPMC5984568.

bioRxiv preprint doi: https://doi.org/10.1101/735449; this version posted August 14, 2019. The copyright holder for this preprint (which was not certified by peer review) is the author/funder, who has granted bioRxiv a license to display the preprint in perpetuity. It is made available under aCC-BY 4.0 International license.

28. The structure of the presenilin 1 (S182) gene and identification of six novel mutations in early onset AD families. Nat Genet. 1995;11(2):219-22. Epub 1995/10/01. doi: 10.1038/ng1095-219. PubMed PMID: 7550356.
29. Hixson JE, Vernier DT. Restriction isotyping of human apolipoprotein E by gene amplification and cleavage with HhaI. J Lipid Res. 1990;31(3):545-8. Epub 1990/03/01. PubMed PMID: 2341813.
30. Franken NA, Rodermond HM, Stap J, Haveman J, van Bree C. Clonogenic assay of cells in vitro. Nat Protoc. 2006;1(5):2315-9. Epub 2007/04/05. doi: 10.1038/nprot.2006.339. PubMed PMID: 17406473.
31. Huang S, Feng C, Wu Y, Yang S, Ma K, Wu X, et al. Dissimilar characteristics of umbilical cord mesenchymal stem cells from donors of different ages. Cell Tissue Bank. 2013;14(4):707-13. Epub 2013/03/12. doi: 10.1007/s10561-013-9364-2. PubMed PMID: 23475054.
32. Xie X, Du X, Li K, Chen Y, Guan Y, Zhao X, et al. Construction of engineered corpus cavernosum with primary mesenchymal stem cells in vitro. Sci Rep. 2017;7(1):18053. Epub 2017/12/24. doi: 10.1038/s41598-017-18129-9. PubMed PMID: 29273785; PubMed Central PMCID: PMCPMC5741727.
33. Sandoval KE, Farr SA, Banks WA, Crider AM, Morley JE, Witt KA. Somatostatin receptor subtype-4 agonist NNC 26-9100 mitigates the effect of soluble Abeta(42) oligomers via a metalloproteinase-dependent mechanism. Brain Res. 2013;1520:145-56. Epub 2013/05/15. doi: 10.1016/j.brainres.2013.05.006. PubMed PMID: 23669069; PubMed Central PMCID: PMCPMC3686878.
34. Stine WB, Jungbauer L, Yu C, LaDu MJ. Preparing Synthetic Aβ in Different Aggregation States. Methods Mol Biol. 2011;670:13-32. doi: 10.1007/978-1-60761-744-0_2. PubMed PMID: 20967580; PubMed Central PMCID: PMC3752843.
35. Armijo E, Gonzalez C, Shahnawaz M, Flores A, Davis B, Soto C. Increased susceptibility to Abeta toxicity in neuronal cultures derived from familial Alzheimer's disease (PSEN1-A246E) induced pluripotent stem cells. Neurosci Lett. 2017;639:74-81. Epub 2016/12/31. doi: 10.1016/j.neulet.2016.12.060. PubMed PMID: 28034781.
36. Pap P, Koszeghy A, Szucs G, Rusznak Z. Cytoplasmic Ca(2+) concentration changes evoked by cholinergic stimulation in primary astrocyte cultures prepared from the rat cochlear nucleus. Hear Res. 2009;255(1-2):73-83. Epub 2009/06/06. doi: 10.1016/j.heares.2009.05.006. PubMed PMID: 19497356.
37. Sekiguchi-Tonosaki M, Obata M, Haruki A, Himi T, Kosaka J. Acetylcholine induces Ca2+ signaling in chicken retinal pigmented epithelial cells during dedifferentiation. Am J Physiol Cell Physiol. 2009;296(5):C1195-206. Epub 2009/02/27. doi: 10.1152/ajpcell.00423.2008. PubMed PMID: 19244481.
38. Lazic SE, Clarke-Williams CJ, Munafo MR. What exactly is 'N' in cell culture and animal experiments? PLoS Biol. 2018;16(4):e2005282. Epub 2018/04/05. doi: 10.1371/journal.pbio.2005282. PubMed PMID: 29617358; PubMed Central PMCID: PMCPMC5902037.
39. Mendivil-Perez M, Velez-Pardo C, Jimenez-Del-Rio M. Neuroprotective Effect of the LRRK2 Kinase Inhibitor PF-06447475 in Human Nerve-Like Differentiated Cells Exposed to Oxidative Stress Stimuli: Implications for Parkinson's Disease. Neurochem Res. 2016;41(10):2675-92. Epub 2016/07/11. doi: 10.1007/s11064-016-1982-1. PubMed PMID: 27394417.
40. Taylor P, Camp S, Radić Z. Acetylcholinesterase. In: Squire LR, editor. Encyclopedia of Neuroscience. Oxford: Academic Press; 2009. p. 5-7.
41. Velez-Pardo C, Ospina GG, Jimenez del Rio M. Abeta[25-35] peptide and iron promote apoptosis in lymphocytes by an oxidative stress mechanism: involvement of H2O2, caspase-3, NF-kappaB, p53 and c-Jun. Neurotoxicology. 2002;23(3):351-65. PubMed PMID: 12387362.

bioRxiv preprint doi: https://doi.org/10.1101/735449; this version posted August 14, 2019. The copyright holder for this preprint (which was not certified by peer review) is the author/funder, who has granted bioRxiv a license to display the preprint in perpetuity. It is made available under aCC-BY 4.0 International license.

42. Fricker M, Tolkovsky AM, Borutaite V, Coleman M, Brown GC. Neuronal Cell Death. Physiol Rev. 2018;98(2):813-80. Epub 2018/03/01. doi: 10.1152/physrev.00011.2017. PubMed PMID: 29488822; PubMed Central PMCID: PMCPMC5966715.
43. Stancu IC, Vasconcelos B, Terwel D, Dewachter I. Models of beta-amyloid induced Tau-pathology: the long and "folded" road to understand the mechanism. Mol Neurodegener. 2014;9:51. Epub 2014/11/20. doi: 10.1186/1750-1326-9-51. PubMed PMID: 25407337; PubMed Central PMCID: PMCPMC4255655.
44. Zhou Y, Shi J, Chu D, Hu W, Guan Z, Gong CX, et al. Relevance of Phosphorylation and Truncation of Tau to the Etiopathogenesis of Alzheimer's Disease. Front Aging Neurosci. 2018;10:27. Epub 2018/02/24. doi: 10.3389/fnagi.2018.00027. PubMed PMID: 29472853; PubMed Central PMCID: PMCPMC5810298.
45. Simic G, Babic Leko M, Wray S, Harrington C, Delalle I, Jovanov-Milosevic N, et al. Tau Protein Hyperphosphorylation and Aggregation in Alzheimer's Disease and Other Tauopathies, and Possible Neuroprotective Strategies. Biomolecules. 2016;6(1):6. Epub 2016/01/12. doi: 10.3390/biom6010006. PubMed PMID: 26751493; PubMed Central PMCID: PMCPMC4808800.
46. Du X, Wang X, Geng M. Alzheimer's disease hypothesis and related therapies. Transl Neurodegener. 2018;7:2. Epub 2018/02/10. doi: 10.1186/s40035-018-0107-y. PubMed PMID: 29423193; PubMed Central PMCID: PMCPMC5789526.
47. Hardy J. The discovery of Alzheimer-causing mutations in the APP gene and the formulation of the "amyloid cascade hypothesis". Febs j. 2017;284(7):1040-4. Epub 2017/01/06. doi: 10.1111/febs.14004. PubMed PMID: 28054745.
48. Doig AJ, Del Castillo-Frias MP, Berthoumieu O, Tarus B, Nasica-Labouze J, Sterpone F, et al. Why Is Research on Amyloid-beta Failing to Give New Drugs for Alzheimer's Disease? ACS Chem Neurosci. 2017;8(7):1435-7. Epub 2017/06/07. doi: 10.1021/acschemneuro.7b00188. PubMed PMID: 28586203.
49. Khachaturian AS, Hayden KM, Mielke MM, Tang Y, Lutz MW, Gustafson DR, et al. Future prospects and challenges for Alzheimer's disease drug development in the era of the NIA-AA Research Framework. Alzheimers Dement. 2018;14(4):532-4. Epub 2018/04/15. doi: 10.1016/j.jalz.2018.03.003. PubMed PMID: 29653605.
50. Sannerud R, Esselens C, Ejsmont P, Mattera R, Rochin L, Tharkeshwar AK, et al. Restricted Location of PSEN2/gamma-Secretase Determines Substrate Specificity and Generates an Intracellular Abeta Pool. Cell. 2016;166(1):193-208. Epub 2016/06/14. doi: 10.1016/j.cell.2016.05.020. PubMed PMID: 27293189.
51. Takahashi RH, Nagao T, Gouras GK. Plaque formation and the intraneuronal accumulation of beta-amyloid in Alzheimer's disease. Pathol Int. 2017;67(4):185-93. Epub 2017/03/07. doi: 10.1111/pin.12520. PubMed PMID: 28261941.
52. Kinumi T, Kimata J, Taira T, Ariga H, Niki E. Cysteine-106 of DJ-1 is the most sensitive cysteine residue to hydrogen peroxide-mediated oxidation in vivo in human umbilical vein endothelial cells. Biochem Biophys Res Commun. 2004;317(3):722-8. doi: 10.1016/j.bbrc.2004.03.110. PubMed PMID: 15081400.
53. Jimenez-Del-Rio M, Velez-Pardo C. The bad, the good, and the ugly about oxidative stress. Oxid Med Cell Longev. 2012;2012:163913. doi: 10.1155/2012/163913. PubMed PMID: 22619696; PubMed Central PMCID: PMCPMC3350994.
54. Cheignon C, Tomas M, Bonnefont-Rousselot D, Faller P, Hureau C, Collin F. Oxidative stress and the amyloid beta peptide in Alzheimer's disease. Redox Biol. 2018;14:450-64. Epub 2017/10/29. doi: 10.1016/j.redox.2017.10.014. PubMed PMID: 29080524; PubMed Central PMCID: PMCPMC5680523.
55. Kaminsky YG, Tikhonova LA, Kosenko EA. Critical analysis of Alzheimer's amyloid-beta toxicity to mitochondria. Front Biosci (Landmark Ed). 2015;20:173-97. Epub 2015/01/02. PubMed PMID: 25553446.

bioRxiv preprint doi: https://doi.org/10.1101/735449; this version posted August 14, 2019. The copyright holder for this preprint (which was not certified by peer review) is the author/funder, who has granted bioRxiv a license to display the preprint in perpetuity. It is made available under aCC-BY 4.0 International license.

56. Di Marzo N, Chisci E, Giovannoni R. The Role of Hydrogen Peroxide in Redox-Dependent Signaling: Homeostatic and Pathological Responses in Mammalian Cells. Cells. 2018;7(10). Epub 2018/10/06. doi: 10.3390/cells7100156. PubMed PMID: 30287799; PubMed Central PMCID: PMCPMC6211135.
57. Saitoh M, Nishitoh H, Fujii M, Takeda K, Tobiume K, Sawada Y, et al. Mammalian thioredoxin is a direct inhibitor of apoptosis signal-regulating kinase (ASK) 1. EMBO J. 1998;17(9):2596-606. doi: 10.1093/emboj/17.9.2596. PubMed PMID: 9564042; PubMed Central PMCID: PMCPMC1170601.
58. Reddy CE, Albanito L, De Marco P, Aiello D, Maggiolini M, Napoli A, et al. Multisite phosphorylation of c-Jun at threonine 91/93/95 triggers the onset of c-Jun pro-apoptotic activity in cerebellar granule neurons. Cell Death Dis. 2013;4:e852. Epub 2013/10/12. doi: 10.1038/cddis.2013.381. PubMed PMID: 24113186; PubMed Central PMCID: PMCPMC3824690.
59. Morishima Y, Gotoh Y, Zieg J, Barrett T, Takano H, Flavell R, et al. Beta-amyloid induces neuronal apoptosis via a mechanism that involves the c-Jun N-terminal kinase pathway and the induction of Fas ligand. J Neurosci. 2001;21(19):7551-60. Epub 2001/09/22. PubMed PMID: 11567045.
60. Lu H, Hou G, Zhang Y, Dai Y, Zhao H. c-Jun transactivates Puma gene expression to promote osteoarthritis. Mol Med Rep. 2014;9(5):1606-12. Epub 2014/02/26. doi: 10.3892/mmr.2014.1981. PubMed PMID: 24566851.
61. Yu J, Zhang L, Hwang PM, Kinzler KW, Vogelstein B. PUMA induces the rapid apoptosis of colorectal cancer cells. Mol Cell. 2001;7(3):673-82. Epub 2001/07/21. PubMed PMID: 11463391.
62. Nakano K, Vousden KH. PUMA, a novel proapoptotic gene, is induced by p53. Mol Cell. 2001;7(3):683-94. Epub 2001/07/21. PubMed PMID: 11463392.
63. Fuchs SY, Adler V, Pincus MR, Ronai Z. MEKK1/JNK signaling stabilizes and activates p53. Proc Natl Acad Sci U S A. 1998;95(18):10541-6. PubMed PMID: 9724739; PubMed Central PMCID: PMCPMC27930.
64. Hikisz P, Kilianska ZM. PUMA, a critical mediator of cell death--one decade on from its discovery. Cell Mol Biol Lett. 2012;17(4):646-69. Epub 2012/09/25. doi: 10.2478/s11658-012-0032-5. PubMed PMID: 23001513.
65. Pena-Blanco A, Garcia-Saez AJ. Bax, Bak and beyond - mitochondrial performance in apoptosis. Febs j. 2018;285(3):416-31. Epub 2017/07/30. doi: 10.1111/febs.14186. PubMed PMID: 28755482.
66. Han XJ, Hu YY, Yang ZJ, Jiang LP, Shi SL, Li YR, et al. Amyloid beta-42 induces neuronal apoptosis by targeting mitochondria. Mol Med Rep. 2017;16(4):4521-8. Epub 2017/08/30. doi: 10.3892/mmr.2017.7203. PubMed PMID: 28849115; PubMed Central PMCID: PMCPMC5647099.
67. Wirths O, Multhaup G, Bayer TA. A modified beta-amyloid hypothesis: intraneuronal accumulation of the beta-amyloid peptide--the first step of a fatal cascade. J Neurochem. 2004;91(3):513-20. Epub 2004/10/16. doi: 10.1111/j.1471-4159.2004.02737.x. PubMed PMID: 15485483.
68. Briggs CA, Chakroborty S, Stutzmann GE. Emerging pathways driving early synaptic pathology in Alzheimer's disease. Biochem Biophys Res Commun. 2017;483(4):988-97. Epub 2016/09/24. doi: 10.1016/j.bbrc.2016.09.088. PubMed PMID: 27659710; PubMed Central PMCID: PMCPMC5303639.
69. Demuro A, Parker I. Cytotoxicity of intracellular abeta42 amyloid oligomers involves Ca2+ release from the endoplasmic reticulum by stimulated production of inositol trisphosphate. J Neurosci. 2013;33(9):3824-33. Epub 2013/03/01. doi: 10.1523/jneurosci.4367-12.2013. PubMed PMID: 23447594; PubMed Central PMCID: PMCPMC3708452.

bioRxiv preprint doi: https://doi.org/10.1101/735449; this version posted August 14, 2019. The copyright holder for this preprint (which was not certified by peer review) is the author/funder, who has granted bioRxiv a license to display the preprint in perpetuity. It is made available under aCC-BY 4.0 International license.

70. Ju Y, Asahi T, Sawamura N. Arctic mutant Abeta40 aggregates on alpha7 nicotinic acetylcholine receptors and inhibits their functions. J Neurochem. 2014;131(5):667-74. Epub 2014/07/26. doi: 10.1111/jnc.12837. PubMed PMID: 25059095.
71. Lasala M, Fabiani C, Corradi J, Antollini S, Bouzat C. Molecular Modulation of Human alpha7 Nicotinic Receptor by Amyloid-beta Peptides. Front Cell Neurosci. 2019;13:37. Epub 2019/02/26. doi: 10.3389/fncel.2019.00037. PubMed PMID: 30800059; PubMed Central PMCID: PMCPMC6376857.
72. Kandel N, Zheng T, Huo Q, Tatulian SA. Membrane Binding and Pore Formation by a Cytotoxic Fragment of Amyloid beta Peptide. J Phys Chem B. 2017;121(45):10293-305. Epub 2017/10/19. doi: 10.1021/acs.jpcb.7b07002. PubMed PMID: 29039658.
73. Avila J. Our Working Point of View of Tau Protein. J Alzheimers Dis. 2018;62(3):1277-85. Epub 2017/10/19. doi: 10.3233/jad-170600. PubMed PMID: 29036830; PubMed Central PMCID: PMCPMC5870002.
74. Zheng WH, Bastianetto S, Mennicken F, Ma W, Kar S. Amyloid beta peptide induces tau phosphorylation and loss of cholinergic neurons in rat primary septal cultures. Neuroscience. 2002;115(1):201-11. Epub 2002/10/29. PubMed PMID: 12401334.
75. Hu X, Li X, Zhao M, Gottesdiener A, Luo W, Paul S. Tau pathogenesis is promoted by Abeta1-42 but not Abeta1-40. Mol Neurodegener. 2014;9:52. Epub 2014/11/25. doi: 10.1186/1750-1326-9-52. PubMed PMID: 25417177; PubMed Central PMCID: PMCPMC4277831.
76. Welikovitch LA, Do Carmo S, Magloczky Z, Szocsics P, Loke J, Freund T, et al. Evidence of intraneuronal Abeta accumulation preceding tau pathology in the entorhinal cortex. Acta Neuropathol. 2018;136(6):901-17. Epub 2018/10/27. doi: 10.1007/s00401-018-1922-z. PubMed PMID: 30362029.
77. Bloom GS. Amyloid-beta and tau: the trigger and bullet in Alzheimer disease pathogenesis. JAMA Neurol. 2014;71(4):505-8. Epub 2014/02/05. doi: 10.1001/jamaneurol.2013.5847. PubMed PMID: 24493463.
78. Ma QL, Yang F, Rosario ER, Ubeda OJ, Beech W, Gant DJ, et al. Beta-amyloid oligomers induce phosphorylation of tau and inactivation of insulin receptor substrate via c-Jun N-terminal kinase signaling: suppression by omega-3 fatty acids and curcumin. J Neurosci. 2009;29(28):9078-89. Epub 2009/07/17. doi: 10.1523/jneurosci.1071-09.2009. PubMed PMID: 19605645; PubMed Central PMCID: PMCPMC3849615.
79. Yarza R, Vela S, Solas M, Ramirez MJ. c-Jun N-terminal Kinase (JNK) Signaling as a Therapeutic Target for Alzheimer's Disease. Front Pharmacol. 2015;6:321. Epub 2016/01/23. doi: 10.3389/fphar.2015.00321. PubMed PMID: 26793112; PubMed Central PMCID: PMCPMC4709475.
80. Kondo T, Asai M, Tsukita K, Kutoku Y, Ohsawa Y, Sunada Y, et al. Modeling Alzheimer's disease with iPSCs reveals stress phenotypes associated with intracellular Abeta and differential drug responsiveness. Cell Stem Cell. 2013;12(4):487-96. Epub 2013/02/26. doi: 10.1016/j.stem.2013.01.009. PubMed PMID: 23434393.
81. Reiman EM, Quiroz YT, Fleisher AS, Chen K, Velez-Pardo C, Jimenez-Del-Rio M, et al. Brain imaging and fluid biomarker analysis in young adults at genetic risk for autosomal dominant Alzheimer's disease in the presenilin 1 E280A kindred: a case-control study. Lancet Neurol. 2012;11(12):1048-56. Epub 2012/11/10. doi: 10.1016/s1474-4422(12)70228-4. PubMed PMID: 23137948; PubMed Central PMCID: PMCPMC4181671.
82. Quiroz YT, Schultz AP, Chen K, Protas HD, Brickhouse M, Fleisher AS, et al. Brain Imaging and Blood Biomarker Abnormalities in Children With Autosomal Dominant Alzheimer Disease: A Cross-Sectional Study. JAMA Neurol. 2015;72(8):912-9. Epub 2015/06/30. doi: 10.1001/jamaneurol.2015.1099. PubMed PMID: 26121081; PubMed Central PMCID: PMCPMC4625544.
83. Jack CR, Jr., Knopman DS, Jagust WJ, Petersen RC, Weiner MW, Aisen PS, et al. Tracking pathophysiological processes in Alzheimer's disease: an updated hypothetical model of dynamic

bioRxiv preprint doi: https://doi.org/10.1101/735449; this version posted August 14, 2019. The copyright holder for this preprint (which was not certified by peer review) is the author/funder, who has granted bioRxiv a license to display the preprint in perpetuity. It is made available under aCC-BY 4.0 International license.

biomarkers. Lancet Neurol. 2013;12(2):207-16. Epub 2013/01/22. doi: 10.1016/s1474-4422(12)70291-0. PubMed PMID: 23332364; PubMed Central PMCID: PMCPMC3622225.

84. LaFerla FM, Green KN, Oddo S. Intracellular amyloid-beta in Alzheimer's disease. Nat Rev Neurosci. 2007;8(7):499-509. Epub 2007/06/07. doi: 10.1038/nrn2168. PubMed PMID: 17551515.

85. Cline EN, Bicca MA, Viola KL, Klein WL. The Amyloid-beta Oligomer Hypothesis: Beginning of the Third Decade. J Alzheimers Dis. 2018;64(s1):S567-s610. Epub 2018/05/31. doi: 10.3233/jad-179941. PubMed PMID: 29843241; PubMed Central PMCID: PMCPMC6004937.

86. Cehlar O, Skrabana R, Revajova V, Novak M. Structural aspects of Alzheimer's disease immunotherapy targeted against amyloid-beta peptide. Bratisl Lek Listy. 2018;119(4):201-4. Epub 2018/04/18. doi: 10.4149/bll_2018_037. PubMed PMID: 29663816.

bioRxiv preprint doi: https://doi.org/10.1101/735449; this version posted August 14, 2019. The copyright holder for this preprint (which was not certified by peer review) is the author/funder, who has granted bioRxiv a license to display the preprint in perpetuity. It is made available under aCC-BY 4.0 International license.

Figure legend

Figure 1. Characterization of WT PSEN1 and PSEN1 E280A WJ-MSCs.

(A-B) Representative images showing the colony-forming units and **(C-D)** adherent growth and fibroblast-like morphology typical of WJ-MSCs. **(E-F)** Karyotype analysis performed at passage 2 showing chromosomal normality (46XX). **(G-H)** Flow cytometry analyses showing the percentage of double-positive CD9/ CD73/ CD90/ CD34 and CD45 WJ-MSCs. **(I, O)** Oil-Red-O negatively stained undifferentiated WJ-MSCs grown on regular culture medium. **(J, P)** Oil-Red-O positively stained adipocytes differentiated from WJ-MSCs showing intracellular red lipidic vacuoles. **(K, Q)** Von Kossa negatively stained undifferentiated WJ-MSCs grown on regular culture medium. **(L, R)** Von Kossa positively stained osteoblasts differentiated from WJ-MSCs showing silver intracellular precipitates. **(M, S)** Toluidine blue negatively stained undifferentiated WJ-MSCs grown on regular culture medium. **(N, T)** Toluidine blue positively stained chondrocytes differentiated from WJ-MSCs showing extracellular glycoprotein matrix. Image magnification, 400x. The images represent 1 out of 3 independent experiments.

Figure 2. Cholinergic-like neurons differentiate from WT PSEN1 and PSEN1 E280A WJ-MSCs.

WT PSEN1 and PSEN1 E280A WJ-MSCs were cultured in cholinergic differentiation medium as described in the *Materials and Methods* section for 4 days. After this time, the proteins in the extracts were blotted with primary antibodies against MAP2, β-tubulin III, GFAP, ChAT and actin proteins. The intensities of the western blot bands shown in **(A)** were measured **(B, C, D, E)** by an infrared imaging system (Odyssey, LI-COR), and the

bioRxiv preprint doi: https://doi.org/10.1101/735449; this version posted August 14, 2019. The copyright holder for this preprint (which was not certified by peer review) is the author/funder, who has granted bioRxiv a license to display the preprint in perpetuity. It is made available under aCC-BY 4.0 International license.

intensity was normalized to that of actin. **(F)** Measurements of acetylcholinesterase activity in WT PSEN1 and PSEN1 E280A ChLNs after 7 days of transdifferentiation**. (G-J)** Cells were double stained as indicated in the figure with primary antibodies against β-tubulin III **(green; G''' and I''')** and GFAP **(red; G'' and I'')** or MAP2 **(green; H''' and J''')** and ChAT **(red; H'' and J'')**. The nuclei were stained with Hoechst 33342 **(blue; G'-J')**. Data are expressed as the mean ± SD; $^{*}p<0.05$; $^{**}p<0.01$; $^{***}p<0.001$. The blots and figures represent 1 out of 3 independent experiments. Image magnification, 200x.

Figure 3. PSEN1 E280A cholinergic-like neurons (ChLNs) show high levels of intracellular $A\beta_{42}$ oligomers and oxidized DJ-1.

Synthetic unaggregated (i.e., monomers) and large oligomeric Aβ42 assemblies were prepared as described in *Material and Methods* section according to Stine et al., 2011 [34]. The ChLNs were obtained as follows. After 7 days of transdifferentiation, WT PSEN1 and PSEN1 E280A ChLNs were left in regular culture medium for 0, 2 and 4 days, as indicated in the figure. After this time, the proteins in the extracts were blotted with primary antibodies against $A\beta_{42}$, oxDJ-1Cys^{106} and actin proteins. The intensities of the western blot bands shown in **(A)** were measured **(B, C)** by an infrared imaging system (Odyssey, LI-COR), and the intensity was normalized to that of actin. Additionally, cells were double stained as indicated in the figure **(D-I)** with primary antibodies against $A\beta_{42}$ **(*red*; D'-I')** and oxDJ-1Cys^{106} **(*green*; D''- I'')**. The nuclei were stained with Hoechst 33342 **(*blue*; D'''- I''')**. **(J)** Quantification of $A\beta_{42}$ fluorescence intensity. **(K)** Quantification of oxDJ-1Cys^{106} fluorescence intensity. Data are expressed as the mean ± SD; $^{*}p<0.05$; $^{**}p<0.01$;

bioRxiv preprint doi: https://doi.org/10.1101/735449; this version posted August 14, 2019. The copyright holder for this preprint (which was not certified by peer review) is the author/funder, who has granted bioRxiv a license to display the preprint in perpetuity. It is made available under aCC-BY 4.0 International license.

$^{***}p<0.001$. The blots and figures represent 1 out of 3 independent experiments. Image magnification, 200x; inset magnification, 800x.

Figure 4. PSEN1 E280A cholinergic-like neurons (ChLNs) show loss of mitochondrial membrane potential ($\Delta\Psi_m$), high levels of intracellular reactive oxygen species (ROS), and fragmentation of DNA.

After 7 days of transdifferentiation, WT PSEN1 and PSEN1 E280A ChLNs were left in regular culture medium for 0, 2 and 4 days, as indicated in the figure. Representative histograms showing $DiOC_6(3)^{low}$ **(A-C)**, DCF+ **(D-F)** and $SubG_1$ **(G-I)** populations from WT PSEN1 (*blue*) and PSEN1 E280A (*Red*) ChLNs. Representative MitoTracker **(J'-O')**, DCF **(J''-O'')**, Hoechst **(J'''-O''')** and merge **(J-O)** pictures of WT PSEN1 and PSEN1 E280A ChLNs. **(P)** Quantification of MitoTracker fluorescence intensity. **(Q)** Quantification of DCF fluorescence intensity. Data are expressed as the mean ± SD; $^{*}p<0.05$; $^{**}p<0.01$; $^{***}p<0.001$. The histograms and figures represent 1 out of 3 independent experiments. Image magnification, 200x.

Figure 5. PSEN1 E280A ChLNs display activation of p53, PUMA, c-JUN and CASPASE-3.

After **7** days of transdifferentiation, WT PSEN1 and PSEN1 E280A ChLNs were left in regular culture medium for 0, 2 and 4 days, as indicated in the figure. After this time, the proteins in the extracts were blotted with primary antibodies against phosphorylated c-JUN (c-JUN), p53, PUMA, CASPASE-3 (CASP-3) and actin proteins. The intensities of the western blot bands shown in **(A)** were measured **(B, C, D and E)** by an infrared imaging system (Odyssey, LI-COR), and the intensity was normalized to that of actin. Additionally,

bioRxiv preprint doi: https://doi.org/10.1101/735449; this version posted August 14, 2019. The copyright holder for this preprint (which was not certified by peer review) is the author/funder, who has granted bioRxiv a license to display the preprint in perpetuity. It is made available under aCC-BY 4.0 International license.

after 4 days, ChLNs were double stained as indicated in the figure **(F-I)** with primary antibodies against p53 **(*green*; F' and G')**, PUMA **(*red*; F'' and G''),** c-JUN **(*green*; H' and I')** and CASP-3 **(*red*; H'' and I'')**. The nuclei were stained with Hoechst 33342 **(*blue*; F'''-I''')**. **(J-M)** Quantification of p53 (**J**), PUMA (**K**), c-JUN (**L**) and CASP-3 (**M**) fluorescence intensity. Data are expressed as the mean ± SD; $^{*}p<0.05$; $^{**}p<0.01$; $^{***}p<0.001$. The blots and figures represent 1 out of 3 independent experiments. Image magnification, 200x.

Figure 6. PSEN1 E280A ChLNs show a reduced functional response to acetylcholine (ACh), low acetylcholinesterase activity and high levels of extracellular $A\beta_{42}$ peptide.

After **7** days of transdifferentiation, WT PSEN1 and PSEN1 E280A ChLNs were left in regular culture medium for 0, 2 and 4 days, as indicated in the figure. **(A)** ELISA quantification of extracellular $A\beta_{42}$ peptide in supernatants. Time-lapse images (0, 10, 20, 30, 40 s) of Ca^{2+} fluorescence in WT PSEN1 and PSEN1 E280A ChLNs after 0 **(B-C)**, 2 **(E-F)** and 4 **(H-I)** days in response to ACh treatment. ACh was puffed into the culture at 10 s (*arrow*). Then, the Ca^{2+} fluorescence of the cells was monitored at the indicated times. Color contrast indicates fluorescence intensity: dark blue < light blue < green < yellow < red. **(D, G, J)** Normalized mean fluorescence signal (ΔF/F) over time from the cells indicating temporal cytoplasmic Ca^{2+} elevation in response to ACh treatment. **(K)** Measurement of acetylcholinesterase activity at 0, 2 and 4 days post transdifferentiation. Data are presented as the means ± SD. $^{*}p<0.05$; $^{**}p<0.01$; $^{***}p<0.001$. The histograms and figures represent 1 out of 3 independent experiments. Image magnification, 400x.

bioRxiv preprint doi: https://doi.org/10.1101/735449; this version posted August 14, 2019. The copyright holder for this preprint (which was not certified by peer review) is the author/funder, who has granted bioRxiv a license to display the preprint in perpetuity. It is made available under aCC-BY 4.0 International license.

Figure 7. PSEN1 E280A ChLNs induce phosphorylation of TAU protein.

After **7** days of transdifferentiation, WT PSEN1 and PSEN1 E280A ChLNs were left untreated **(A-I)** or treated with 1 μM JNK inhibitor SP600125 **(J-R)** in regular culture medium for 0, 2 and 4 days as indicated in the figure. After this time, the proteins in the extracts were blotted with primary antibodies against phosphorylated TAU (p-TAU), total TAU (t-TAU) and actin proteins. The intensities of the western blot bands shown in **(A or J)** were measured **(B or K)** by an infrared imaging system (Odyssey, LI-COR), and the p-TAU/t-TAU ratio was normalized to that of actin. Additionally, ChLNs were double stained as indicated in the figure **(C-H or L-Q)** with primary antibodies against p-TAU **(*green*; C'-H' or L'-Q')** and t-TAU **(*red*; C''-H'' or L''-Q'')**. The nuclei were stained with Hoechst 33342 **(*blue*; C'''-H''' or L'''-Q''')**. **(I and R)** Quantification of the p-TAU/ t-TAU fluorescence ratio. Data are expressed as the mean ± SD; $^{*}p<0.05$; $^{**}p<0.01$; $^{***}p<0.001$. The blots and figures represent 1 out of 3 independent experiments. Image magnification, 200x.

Figure 8. Schematic effects of the $A\beta_{42}$ peptide in mutant PSEN1 E280A ChLNs.

(See text for explanation).

bioRxiv preprint doi: https://doi.org/10.1101/735449; this version posted August 14, 2019. The copyright holder for this preprint (which was not certified by peer review) is the author/funder, who has granted bioRxiv a license to display the preprint in perpetuity. It is made available under aCC-BY 4.0 International license.

Cholinergic-like neurons carrying PSEN1 E280A mutation from familial Alzheimer's disease reveal intraneuronal Aβ42 peptide accumulation, hyperphosphorylation of TAU, oxidative stress, apoptosis and Ca2+ flux dysregulation: Therapeutic Implications

Viviana Soto-Mercado[1], Miguel Mendivil-Perez[1], Carlos Velez-Pardo [1], Francisco Lopera[1], Marlene Jimenez-Del-Rio[1,*]

Supplementary Material

Supplementary Figure 1. WT PSEN1 and PSEN1 E280A WJ-MSCs show similar levels of intracellular $A\beta_{42}$ and oxidized DJ-1.

WT PSEN1 and PSEN1 E280A WJ-MSCs were left in regular culture medium for 4 days. Then, the proteins in the extracts and control extracts were blotted with primary antibodies against $A\beta_{42}$, oxDJ-1Cys^{106} and actin proteins. The intensities of the western blot bands shown in **(A)** were measured **(B, C)** by an infrared imaging system (Odyssey, LI-COR), and the intensity was normalized to that of actin. Control lysates were included to validate the results. Additionally, after 0, 2 and 4 days, WJ-MSCs were double stained as indicated in the figure **(D-I)** with primary antibodies against $A\beta_{42}$ **(*red*; D'-I')** and oxDJ-1Cys^{106} **(*green*; D'-I'')**. The nuclei were stained with Hoechst 33342 **(blue; D'''-I''')**. **(J)** Quantification of $A\beta_{42}$ fluorescence intensity. **(K)** Quantification of oxDJ-1Cys^{106} fluorescence as MFI. Data are expressed as the mean ± SD; $^{*}p<0.05$; $^{**}p<0.01$; $^{***}p<0.001$. The blots and figures represent 1 out of 3 independent experiments. Image magnification, 200x.

bioRxiv preprint doi: https://doi.org/10.1101/735449; this version posted August 14, 2019. The copyright holder for this preprint (which was not certified by peer review) is the author/funder, who has granted bioRxiv a license to display the preprint in perpetuity. It is made available under aCC-BY 4.0 International license.

Supplementary Figure 2. WT PSEN1 and PSEN1 E280A WJ-MSCs show similar levels of mitochondrial membrane potential ($\Delta\Psi_m$), intracellular reactive oxygen species (ROS) and DNA fragmentation.

Representative histograms showing $DiOC_6(3)^{low}$ **(A)**, DCF+ **(B)** and $SubG_1$ **(C)** populations from WT PSEN1 (blue) and PSEN1 E280A (Red) WJ-MSCs after 4 days. Representative MitoTracker **(D'-I')**, DCF **(D''-I''),** Hoechst **(D'''-I''')** and merged **(D-I)** pictures of WT PSEN1 and PSEN1 E280A WJ-MSCs after 0, 2 and 4 days. **(J)** Quantification of MitoTracker fluorescence intensity. **(K)** Quantification of DCF fluorescence intensity. Data are expressed as the mean ± SD; $^{*}p<0.05$; $^{**}p<0.01$; $^{***}p<0.001$. The histograms and figures represent 1 out of 3 independent experiments. Image magnification, 200x.

bioRxiv preprint doi: https://doi.org/10.1101/735449; this version posted August 14, 2019. The copyright holder for this preprint (which was not certified by peer review) is the author/funder, who has granted bioRxiv a license to display the preprint in perpetuity. It is made available under aCC-BY 4.0 International license.

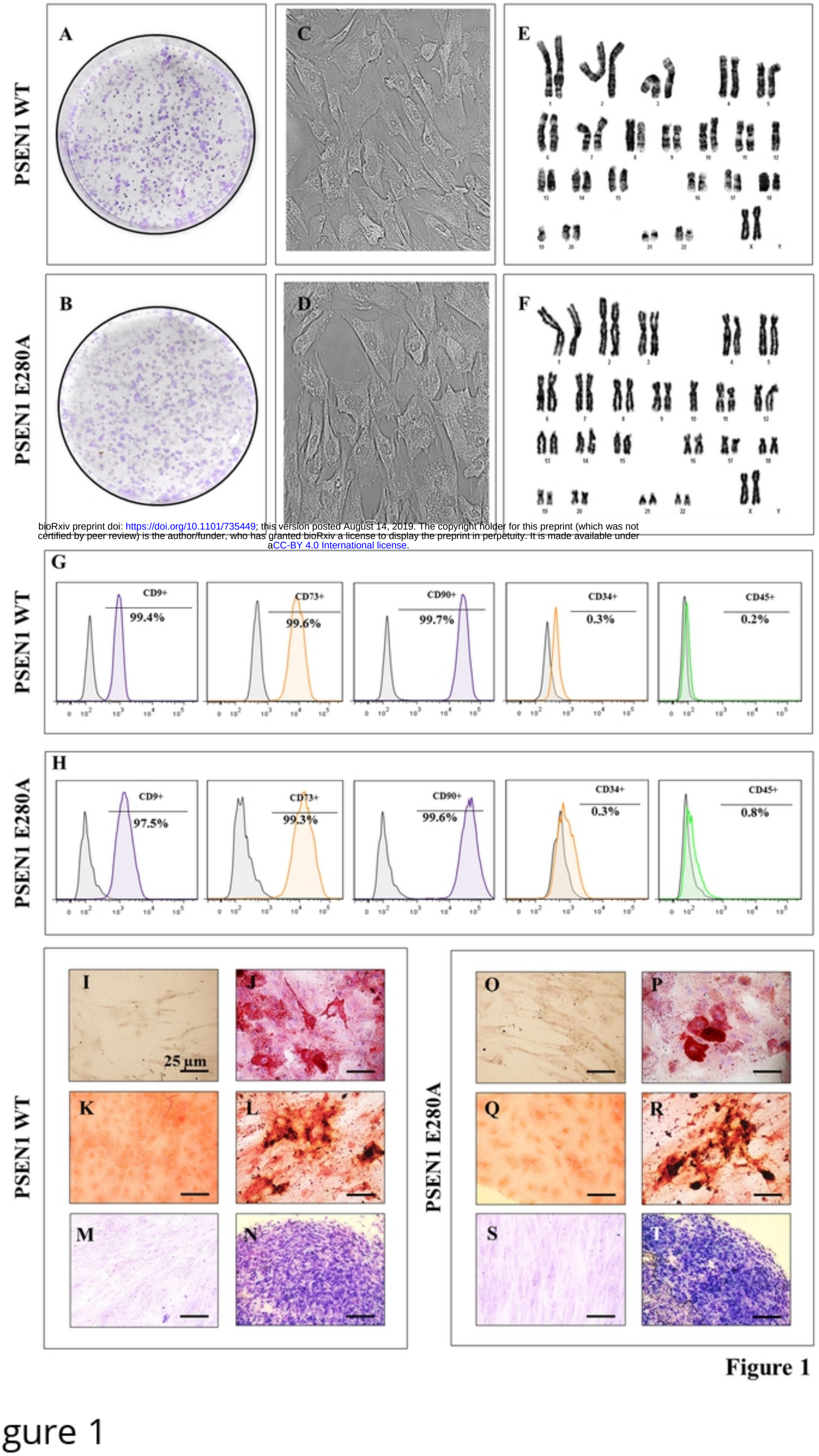

Figure 1

Figure 1

bioRxiv preprint doi: https://doi.org/10.1101/735449; this version posted August 14, 2019. The copyright holder for this preprint (which was not certified by peer review) is the author/funder, who has granted bioRxiv a license to display the preprint in perpetuity. It is made available under aCC-BY 4.0 International license.

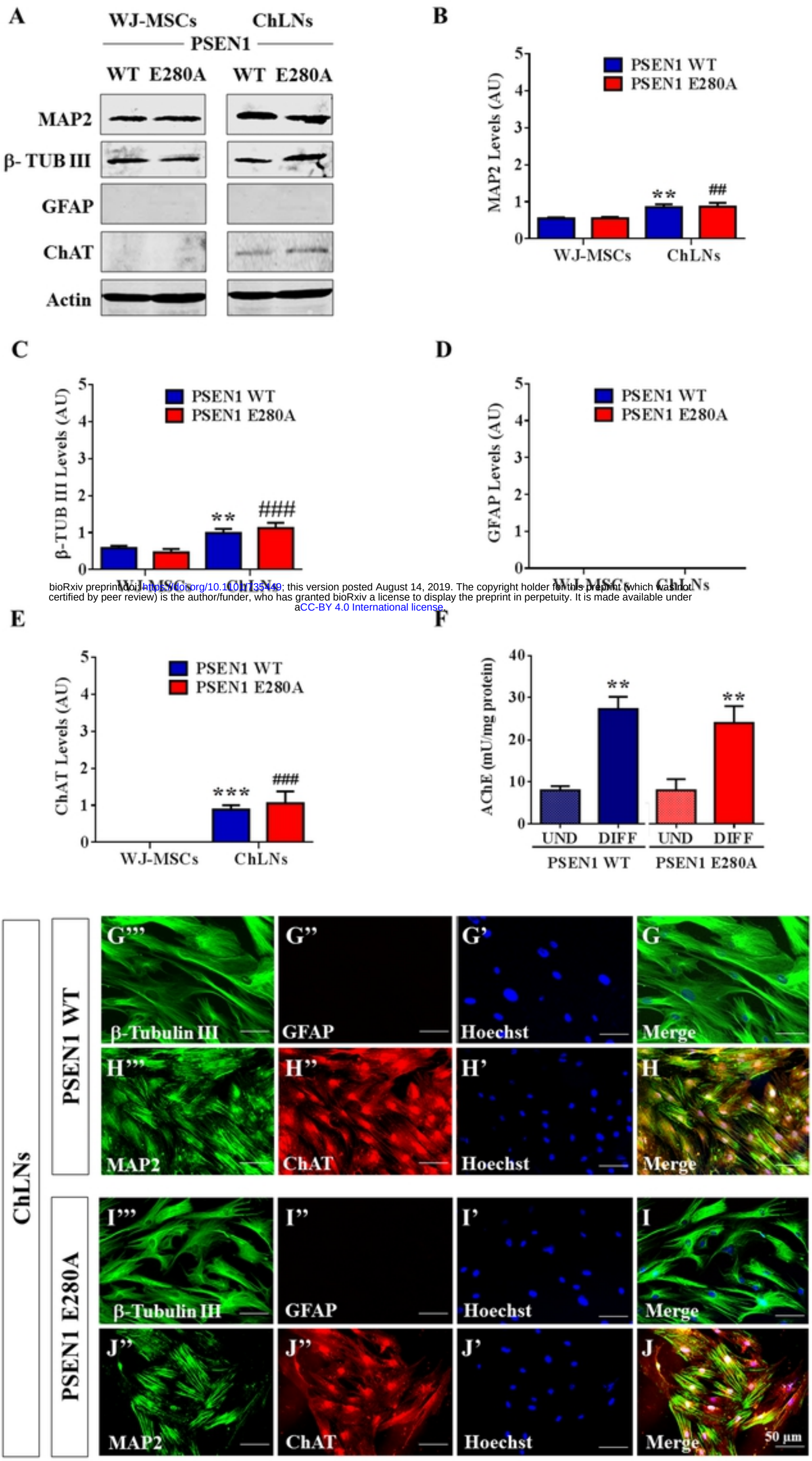

Figure 2

Figure 2

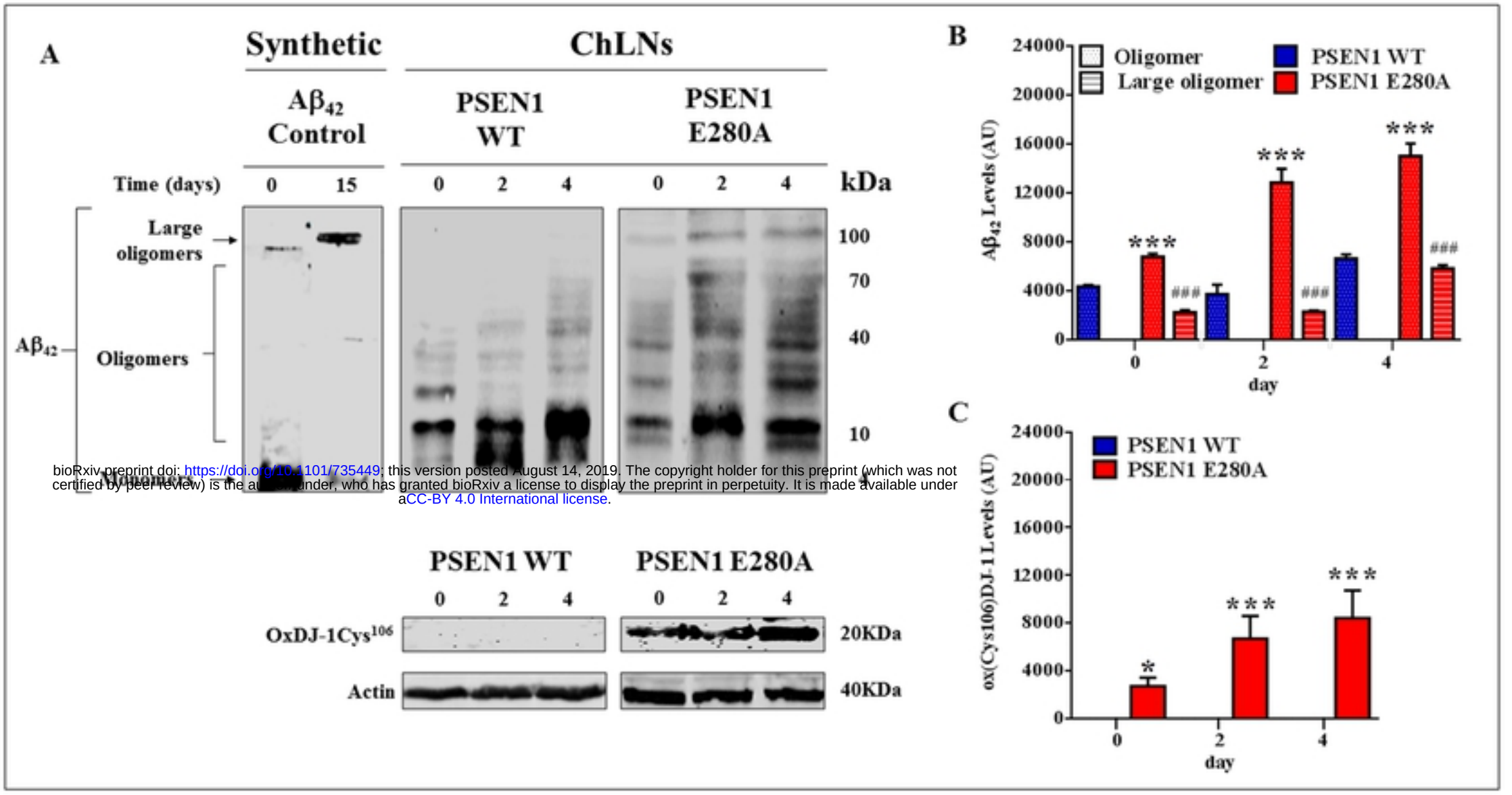

bioRxiv preprint doi: https://doi.org/10.1101/735449; this version posted August 14, 2019. The copyright holder for this preprint (which was not certified by peer review) is the author/funder, who has granted bioRxiv a license to display the preprint in perpetuity. It is made available under aCC-BY 4.0 International license.

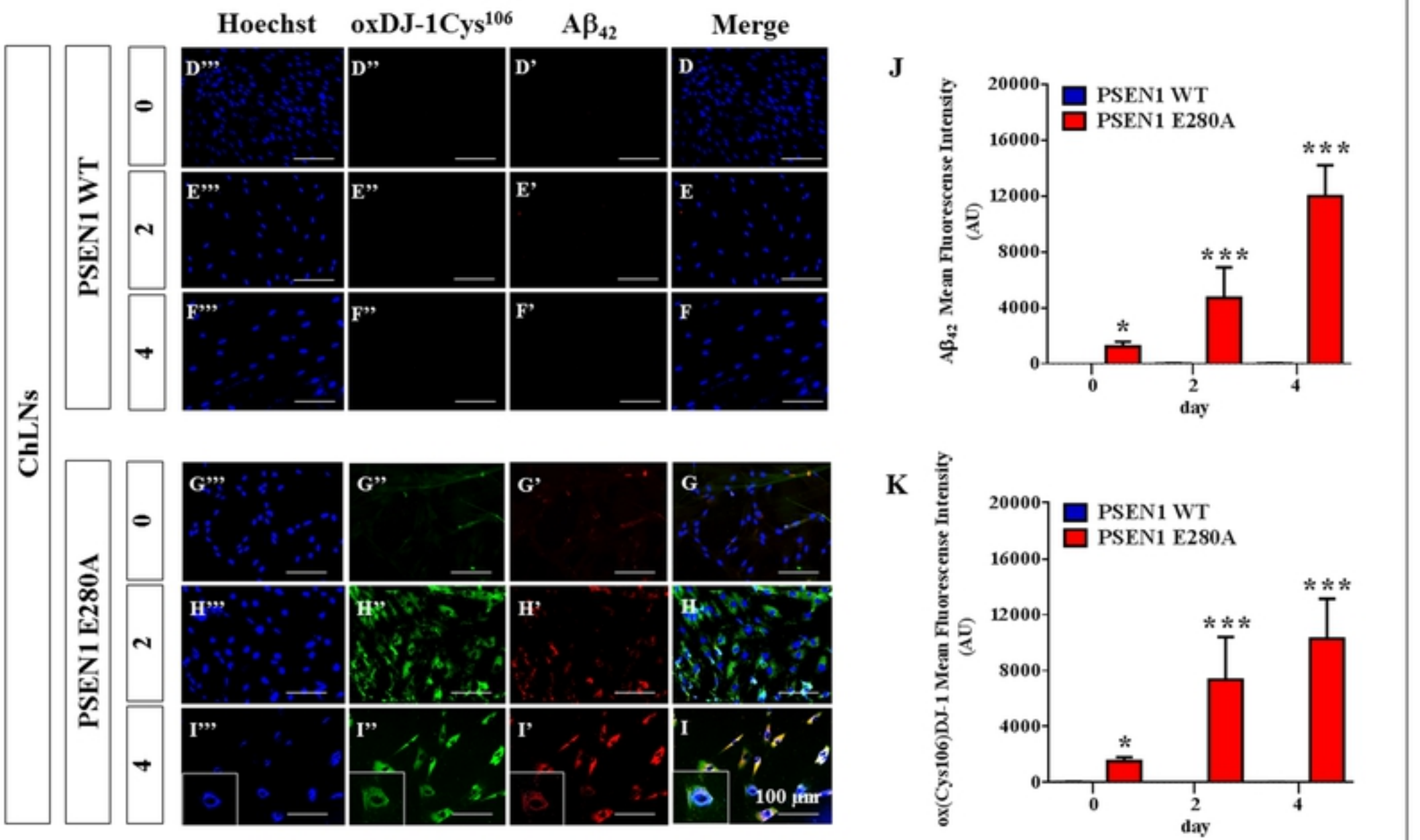

Figure 3

Figure 3

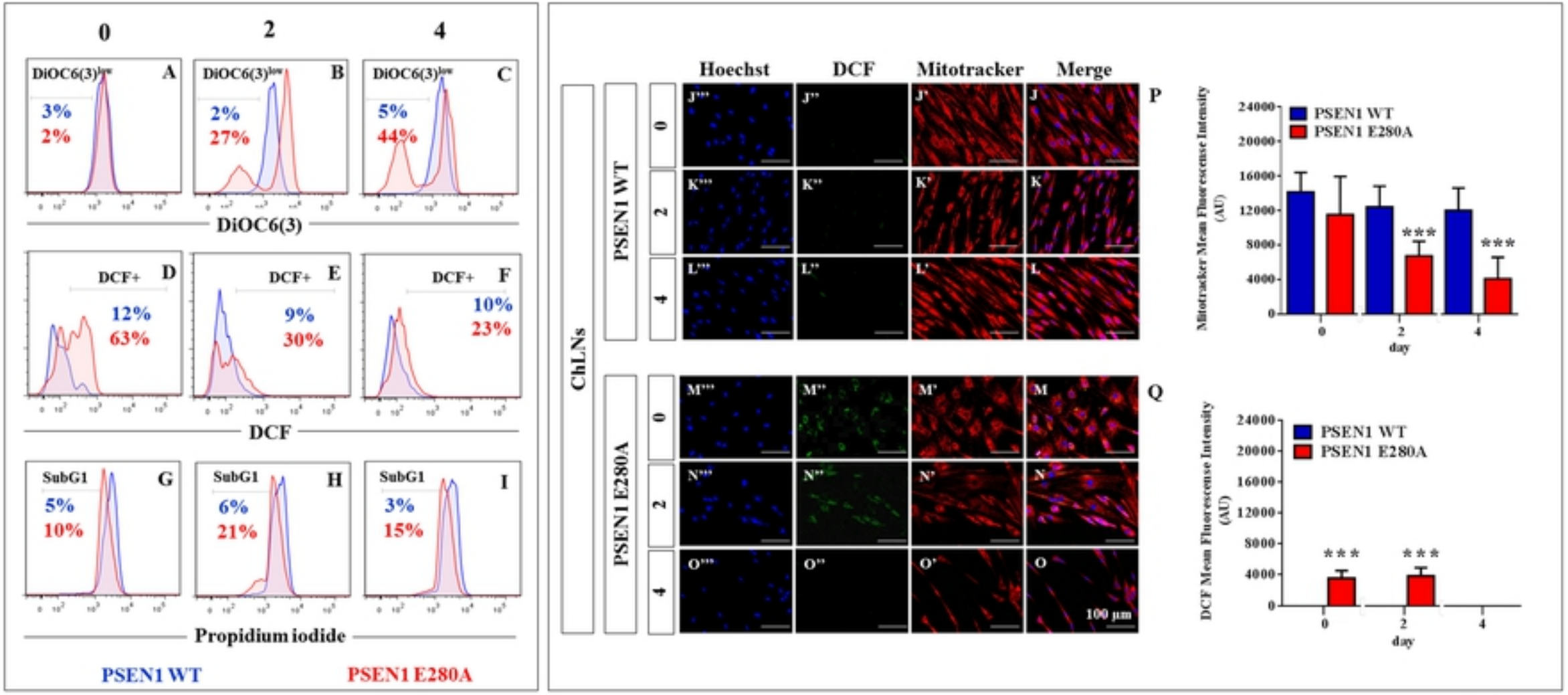

Figure 4

Figure 4

bioRxiv preprint doi: https://doi.org/10.1101/735449; this version posted August 14, 2019. The copyright holder for this preprint (which was not certified by peer review) is the author/funder, who has granted bioRxiv a license to display the preprint in perpetuity. It is made available under aCC-BY 4.0 International license.

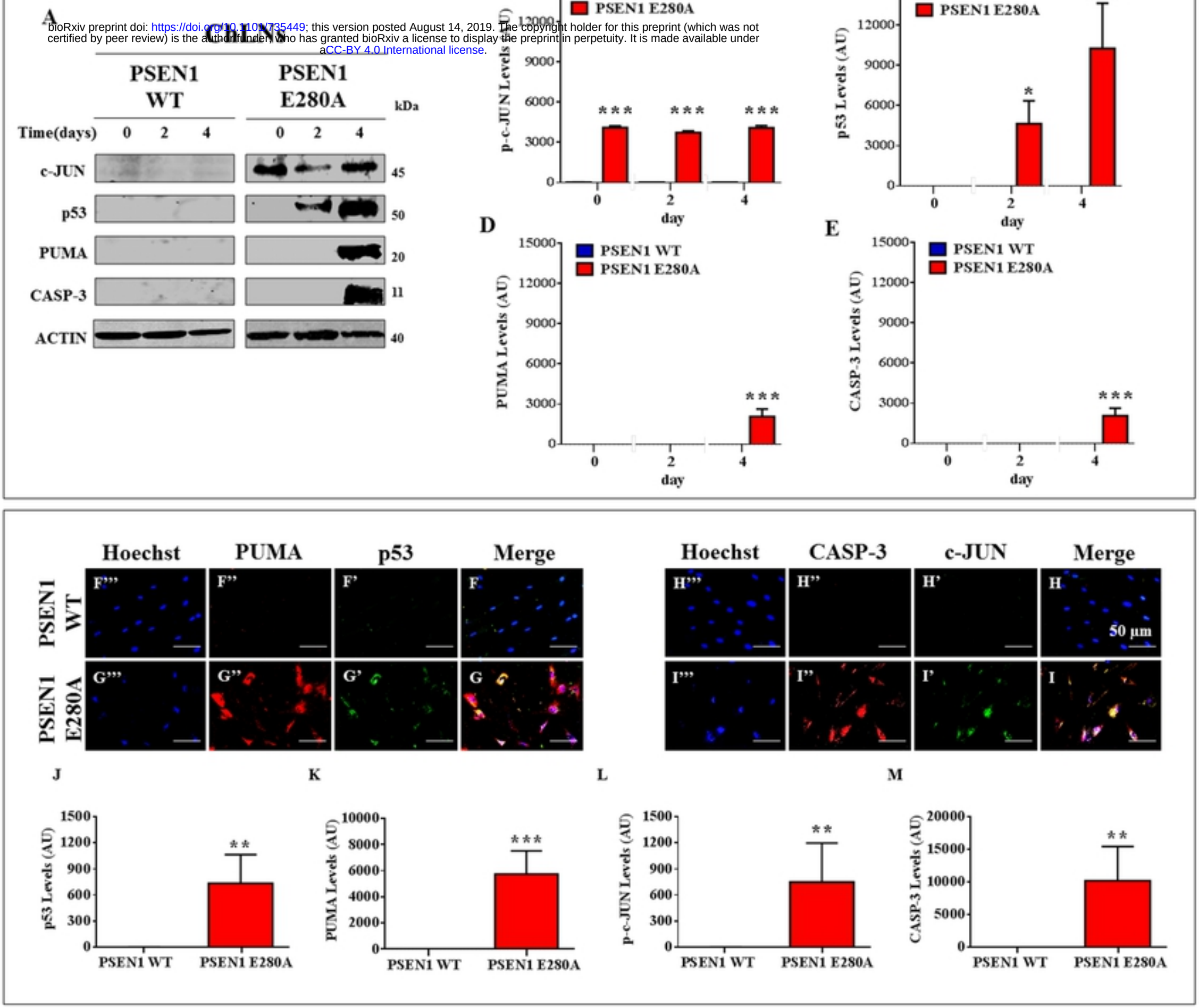

Figure 5

Figure 5

bioRxiv preprint doi: https://doi.org/10.1101/735449; this version posted August 14, 2019. The copyright holder for this preprint (which was not certified by peer review) is the author/funder, who has granted bioRxiv a license to display the preprint in perpetuity. It is made available under a CC-BY 4.0 International license.

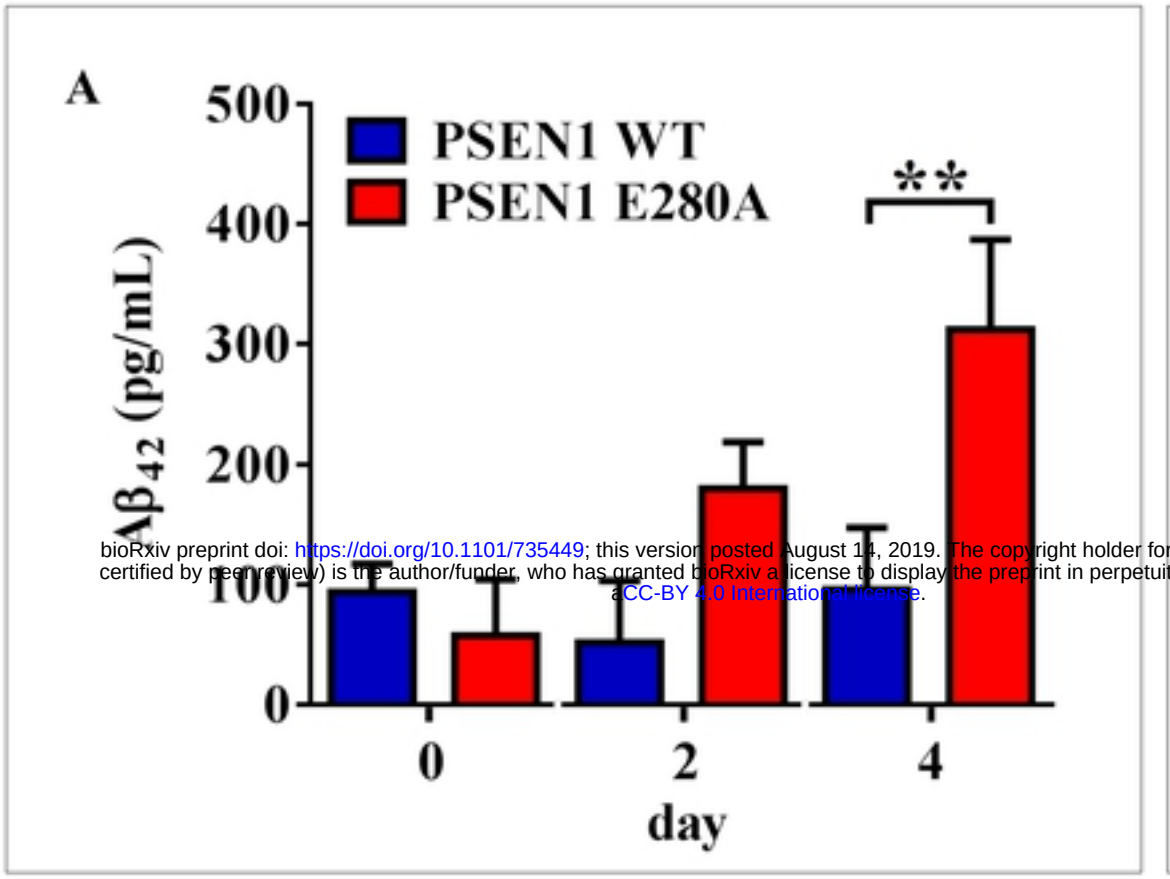

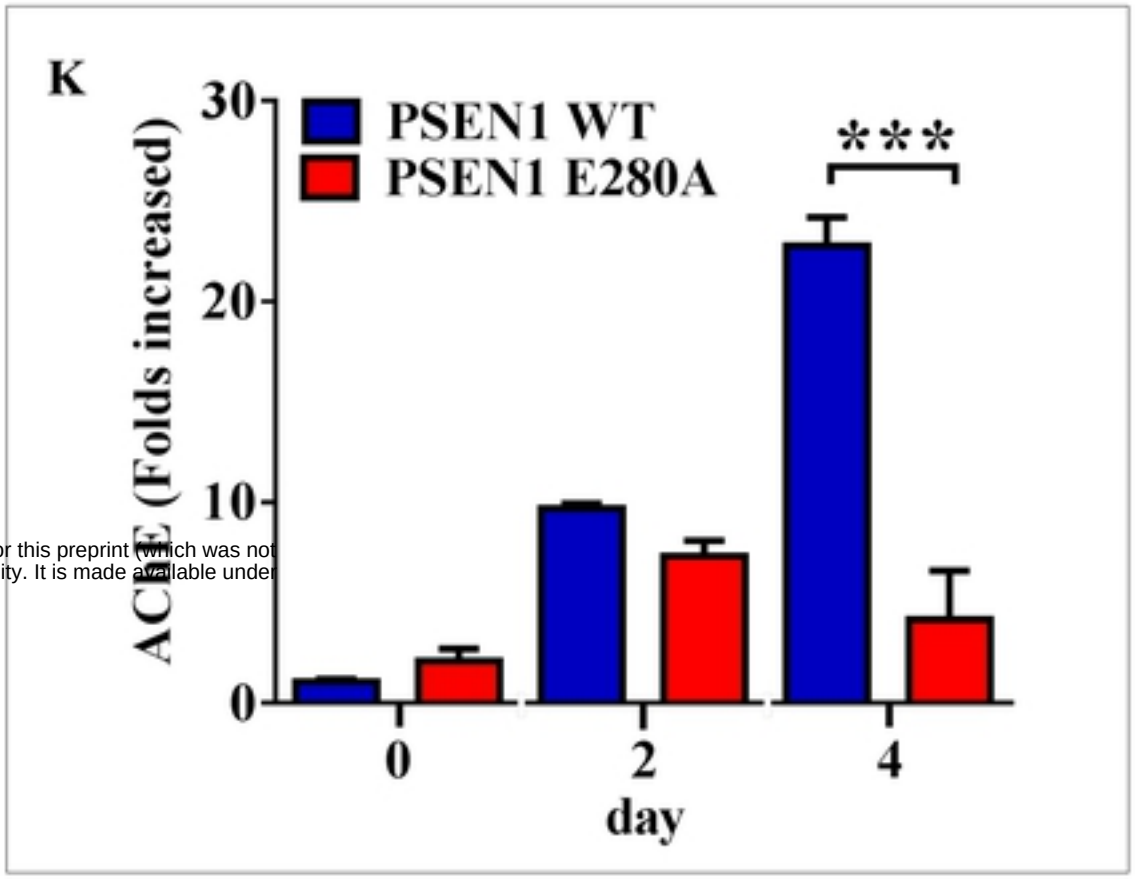

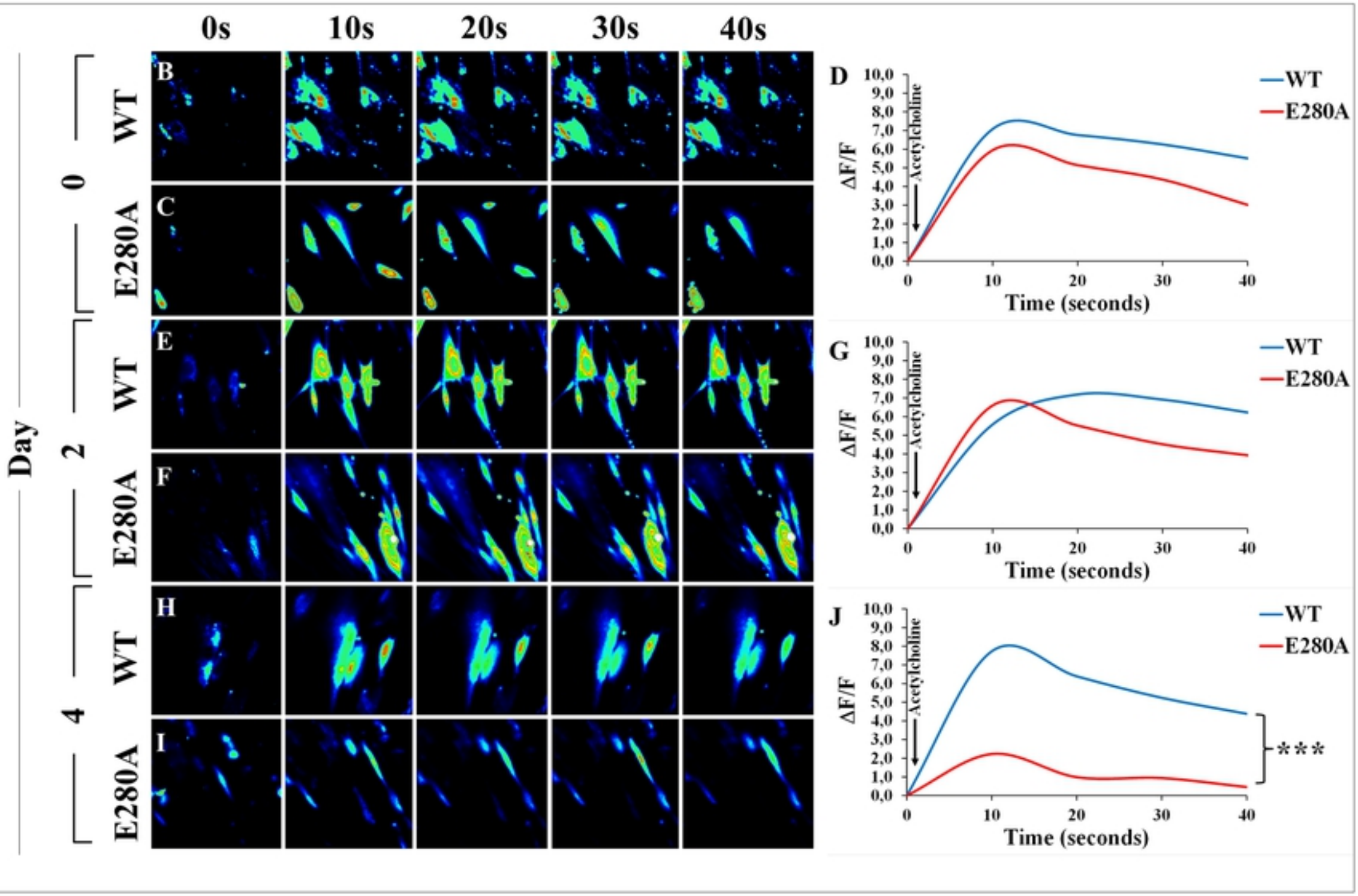

Figure 6

Figure 6

bioRxiv preprint doi: https://doi.org/10.1101/735449; this version posted August 14, 2019. The copyright holder for this preprint (which was not certified by peer review) is the author/funder, who has granted bioRxiv a license to display the preprint in perpetuity. It is made available under aCC-BY 4.0 International license.

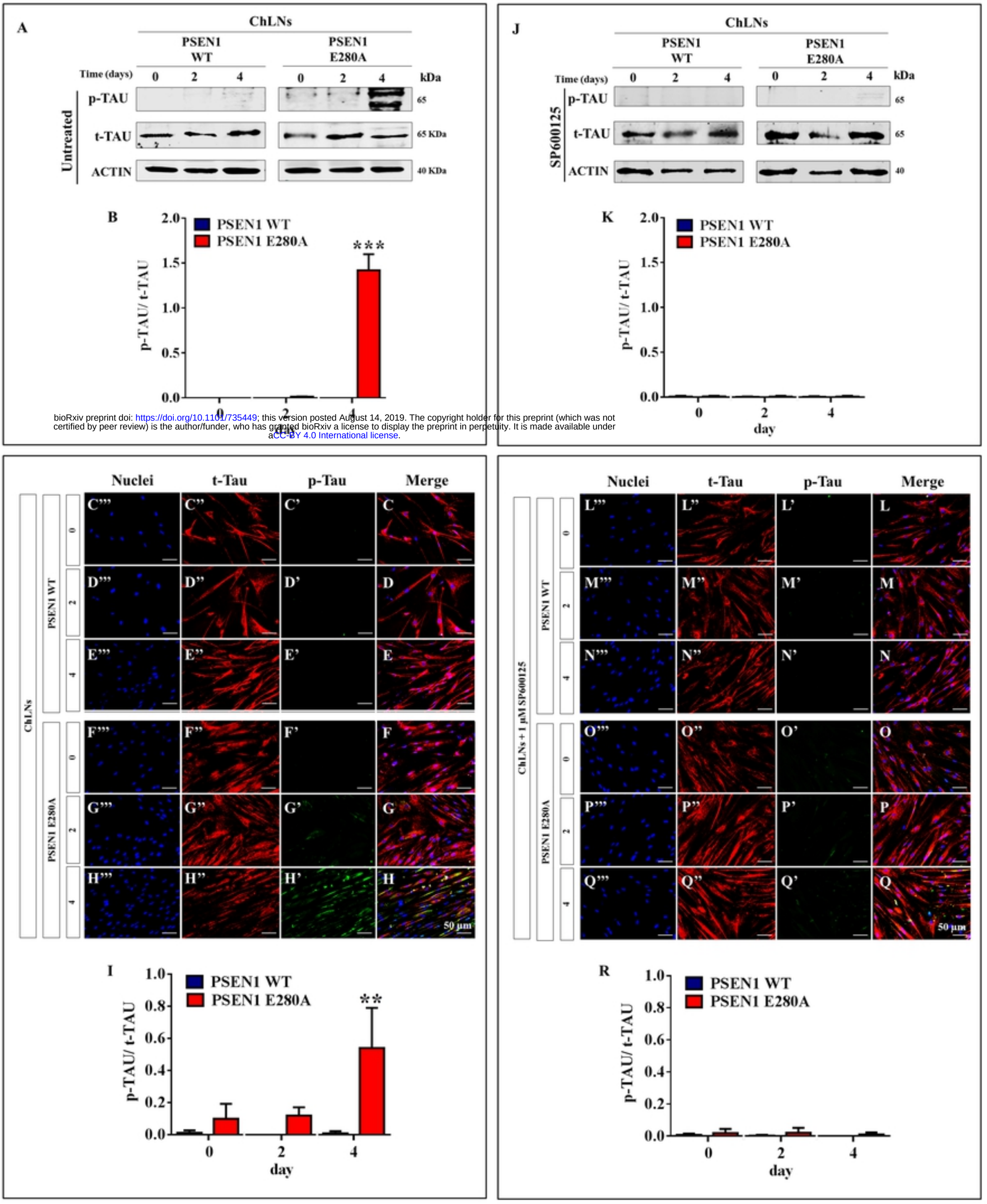

Figure 7

Figure 7

bioRxiv preprint doi: https://doi.org/10.1101/735449; this version posted August 14, 2019. The copyright holder for this preprint (which was not certified by peer review) is the author/funder, who has granted bioRxiv a license to display the preprint in perpetuity. It is made available under aCC-BY 4.0 International license.

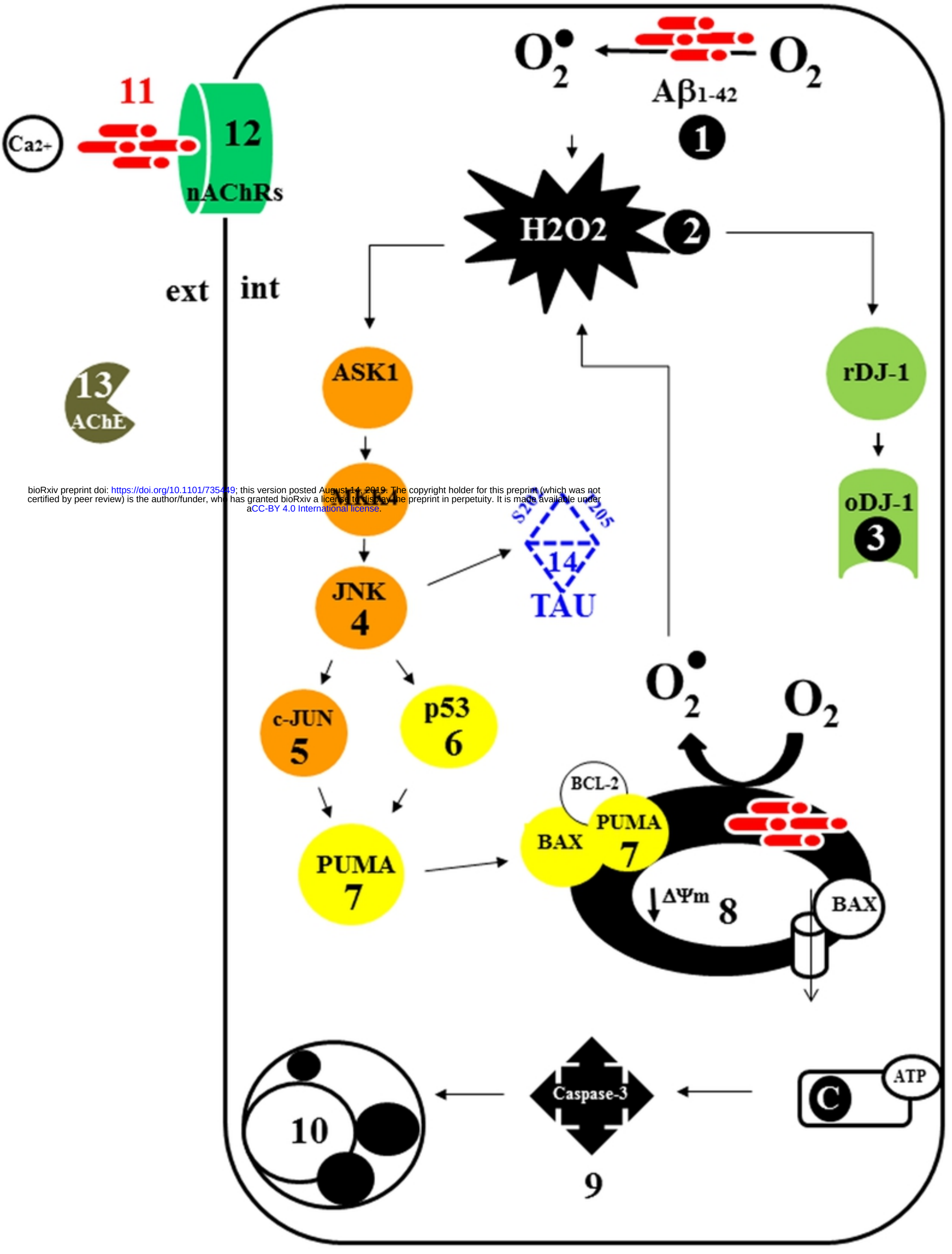

Figure 8

Figure 8